Limiting Efficiency Of Perovskite Solar Cells

By

Ugwuoke, Luke Chinedu

ID No.:40342

Supervised By:

Professor Omololu Akin-Ojo

African University Of Science And Technology
www.aust.edu.ng
P.M.B 681, Garki, Abuja F.C.T
Nigeria.

December, 2014

Limiting Efficiency Of Perovskite Solar Cells

A Thesis

Presented To The Department Of

Theoretical Physics,

African University Of Science And Technology

In Partial Fulfillment Of The Requirements

For The Degree Of

MASTER OF SCIENCE

By

Ugwuoke, Luke Chinedu

Abuja, Nigeria

December, 2014

Limiting Efficiency of Perovskite Solar Cells

By

Ugwuoke, Luke Chinedu

A Thesis Approved By

The Theoretical Physics Department

Recommended: .....
Supervisor: Professor Omololu Akin-Ojo

Approved: .....
Chief Academic Officer

Abstract

The power conversion efficiency of perovskite solar cells has risen from as low as 3.8% to as high as 19.3% in just five years with yet a projected value of over 20% in the next few years by experimentalists. Such a tremendous breakthrough is one of its kind in photo-voltaic research with thin film solar cells as the only major competitor. The light harvesting layer in these new devices has a crystalline structure called the *perovskite structure* which is capable of absorbing photons in both the visible and near infra-red regions of the solar radiation spectrum. In this study, we carried out theoretical studies based on the detailed balance theory originally proposed by Shockley and Queisser, and on a semi-emperical approach based on measured optical absorption spectrum of the three most widely used perovskite absorbers: $CH_3NH_3SnI_3$, $CH_3NH_3PbI_3$, and $CH_3NH_3PbI_{3-x}Cl_x$. We arrived at an upper conversion efficiency limit for a single planar hetero-junction(PHJ) perovskite solar cell with anti-reflection capabilities considering radiative losses as the only carrier loss mechanism within the cell. The limiting efficiency was found to be 29.2% for $CH_3NH_3PbI_3$, 27.5% for $CH_3NH_3PbI_{3-x}Cl_x$, and 24.8% for $CH_3NH_3SnI_3$ under AM1.5 solar spectrum. Issues such as the effect of exciton diffusion length and absorber thickness on the efficiency are also discussed.

Acknowledgements

I thank God for all his blessings of providing me good health, and nice people around me throughout this program .

My profound gratitude goes to NMI(Nelson Mandela Institutions) for the scholarship that allowed me to study at AUST.

I am grateful to my supervisor Prof. Omololu Akin-Ojo, whose encouragement, guidance, and tutoring from the initial to the final level enabled me to develop an understanding of this work. Also, for helping me learn more about Fortran, Octave, Matlab, Latex, and how to get acquainted with the Linux environment; my thanks goes to my supervisor, Bruno Dangross, and Joseph Asare.

All unreferenced sketches in this work was done by me. The octave and fortran codes were written and compiled by me and my supervisor as well as some of the necessary derivations.

Dedication

I dedicate this project to my beloved mum; Mrs Catherine Ugwuoke, and my grandmother; Mrs Josephine Ugwuoke. (May their souls rest in perfect peace).

Also, my dedication goes to my dad; Mr Godwin Ugwuoke, and to all my uncles, brothers, sisters, and friends for their caring and support during my stay at the African University of Science and Technology (AUST), and finally to all those who have contributed immensely in the search for green energy.

Contents

CHAPTER 1

Introduction

"The dye-sensitized solar cell is a photo-voltaic converter that mimics natural photosynthesis. Like green plants and algae, it uses a molecular absorber; the dye, to harvest sunlight and generate electric charges"

Michael Gratzel

1.1 Excitons

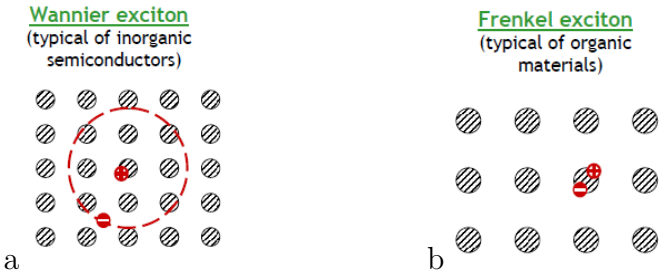

Figure 1.1: Excitons in inorganic and organic semiconductors [40]

An exciton is a bound state of an electron and an electron-hole held together by the Coulombic interaction. It is a quantum mechanical particle found in both organic (e.g; in the dye mentioned above), and inorganic semiconductors (e.g; silicon). The binding energy of an exciton which is the minimum energy required to split the exciton into an individual electron-hole pair can give useful insights on whether a semiconductor will be

rewardful as a photon absorber for photo-voltaic applications in addition to other required optical properties. For instance, in inorganic semiconductors, the exciton binding energy is $\approx$ 10meV, and the electron-hole separation is $\approx 10nm$ Fig.(1.1a); with exciton diffusion lengths of the order of $\approx 50nm - 100nm$. These are called *Wannier excitons* [19]. However, organic semiconductors such as polymer blends are made of *Frenkel excitons* with binding energies of the order of $\approx$ 1eV, electron-hole separation of the order of $\approx 1nm$ Fig.(1.1b); and diffusion lengths of the order of $\approx 10nm$ [27]. This implies that the in-built electric field generated at the pn junction can easily split excitons of the Wannier type; while their longer diffusion lengths enable for almost complete extraction at the electrodes as opposed to the Frenkel type.

In an organic-inorganic hybrid semiconductor such as methylammonium lead tri-iodide ($CH_3NH_3PbI_3$), only Wannier type excitons exist with diffusion lengths in order of $\approx 1\mu m$ which is favourable for absorber thicknesses in the range of $\leq 100nm$. Besides, the exciton lifetime in $CH_3NH_3PbI_3$ powder is high, up to $10ns$ [27]. The combination of these two effects means that the excitons in the $CH_3NH_3PbI_3$ film can travel a longer distance before decay, increasing their likelihood of reaching the hetero-junction to dissociate into free electron–hole pairs.
The origin of high efficiency in perovskite solar cells is therefore a combination of its excellent light absorbing properties; which we intend to explore in chapter three of this study, and the presence of these Wannier excitons.

1.2 The perovskite Solar Cell

Ever since the discovery of the photo-voltaic effect by the French Physicist Edmond Becquerel in 1839, a myriad of emerging solar technologies have been developed, with three of the most heavily researched being organic photo-voltaics (OPVs), dye-sensitized solar cells (DSSCs), and recently, perovskite solar cells.

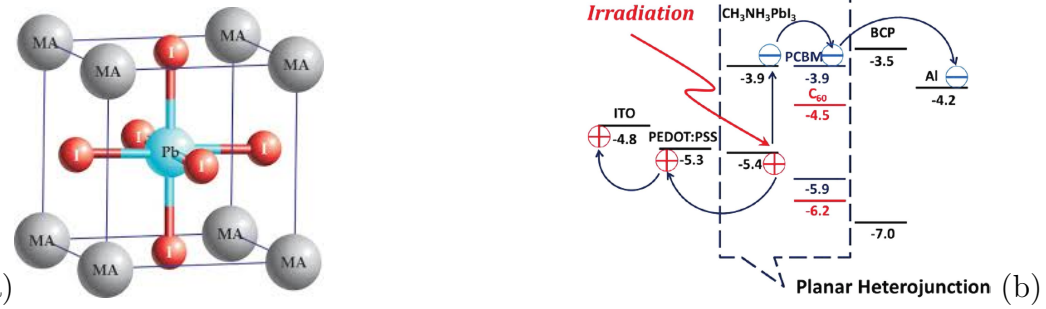

(a) (b)

Figure 1.2: (a) Tetragonal structure of $CH_3NH_3PbI_3$, MA: methylammonium ion, Pb: Pb^{+2} ion, and I: I^- ion. (b) Schematic of a planar hetero-junction perovskite solar cell.[7]

In 2013, Michael Gratzel and his group of energy scientists reported a power conversion efficiency of 12.0% in a planar hetero-junction DSSC by replacing the dye with a methyl ammonium lead iodide ($CH_3NH_3PbI_3$) perovskite [1]. This solar cell is now called a MAPI cell The light absorbing layer in perovskite solar cells is a family of organo-metal based halide perovskite with the general molecular formula; RNH_3BX_3. R is an alkyl group with general formula; C_nH_{2n+1}(usually methyl), B is a group 14 metal (usually Pb or Sn), and X is a halogen (usually I, Cl, Br or mixed). On the other hand, the perovskite as a crystal structure have been found to exist in three different phases namely cubic, tetragonal and orthorhombic. The most stable phases being the tetragonal and cubic exist at room temperature and above while the least stable orthorhombic phase exists at low temperatures [9].

In most planar hetero-junction perovskite solar cells, the perovskite can play both the role of a light absorber and a hole transport layer (HTL) [7]. The perovskite can also be sandwiched between a HTL and an electron transport layer (ETL) [1, 8]. The HTL is a p-type semiconductor that only allows holes to be transported across it, while the ETL is an n-type semiconductor that only allows electrons to be transported across it; Fig.(1.2b). The band gap alignments are such that carrier transport and extraction is enhanced. The work functions of the metals used as cathode(Al) and anode(ITO-indium tin oxide); Fig.(1.2b), are such that charge collection quickly occurs. The current density of the solar cell is determined by the absorption spectrum of the perovskite-light absorbing layer which generates free electron-hole pair under irradiation.

The power conversion efficiency(PCE) of a hetero-junction perovskite solar cell is limited by several factors. These factors ranges from carrier recombination losses such as radiative recombination of electron-hole pairs, non-radiative recombination due to interstitial defects and defects within the perovskite that can act as traps for electrons and holes, Auger recombination, losses at the hetero-junction interface due to band gap misalignment and charge extraction and collection losses at the ohmic contacts [1, 6, 7, 8]. However, the most predominant of these losses is radiative, leading to high radiative efficiency observed in MAPI cells [6]. [1]

1.3 Planckian Spectrum

The wave-particle duality of light allows us to treat photons as particles of light. Photons travel with speed of light c_0 in vacuum and with speed c in a material of refractive index n; where $c = c_0/n$. To describe quantum-like transport of particles, we need to treat photons as bosons in accordance with quantum statistical mechanics.
A blackbody is a non-reflecting body which completely absorbs all photon energies $\hbar\omega = E$

[1]Note that section (1.2) was only meant to serve as an introduction to the topic and does not in any form explain all the features of the perovskite solar cell available in scientific literatures. Section (1.3) introduces the concept of blackbody radiation which is also clearly elucidated in Wurfels' book [5]

incident on it. Hence, it has unity absorptivity: $a(E) = 1$. An approximate example is the sun. The Planckian spectrum describes the photon density $dn(E)$ in a blackbody cavity for photon energies between E and $E + dE$. This is given by:

$$dn(E) = D(E)f(E)dE \tag{1.1}$$

where $D(E)$ is the photon density of states (number of states per unit volume per energy interval dE) which the photons can occupy. $f(E)$ is the probability of occupation which determines the distribution of photons over the states as a function of the energy E. According to Bose-Einstein statistics, $f(E)$ is given by:

$$f(E) = \frac{1}{exp(\frac{E-\mu}{kT}) - 1} \tag{1.2}$$

where $k = 8.617 \times 10^{-5} ev/K$ is the Boltzmann constant, T is the blackbody temperature; and μ is the chemical potential of the photon which is zero for both thermal and solar radiation [5].

To find the density of states $D(E)$, we recall that in phase space, a state in the cavity has a volume: $h^3 = \Delta x \Delta p_x \Delta y \Delta p_y \Delta z \Delta p_z$ in accordance with Heisenberg's Uncertainty principle. In such a cavity, photons are delocalized such that: $\Delta x \Delta y \Delta z = L_x L_y L_z = V$; which is the volume of the cavity. Similarly, $\Delta P_x \Delta P_y \Delta p_z = \Delta p^3 = h^3/V$.

However, due to the polarization of light in two perpendicular directions, each volume Δp^3 therefore contains two photon states. All states in which the photons have energies $E' < E$ lie in a sphere of radius $|\vec{p}|$=E/c. The number of such states per unit volume is: $N/V = 2 \times (\frac{4\pi p^3}{3})/h^3 = \frac{8\pi E^3}{3(hc)^3}$.

Hence, $d(N/V) = \frac{8\pi E^2}{(hc)^3} dE \Rightarrow D(E) = \frac{d(N/V)}{dE} = \frac{8\pi E^2}{(hc)^3}$. For a spherical cavity, photons within it exhibit isotropic motion. Assuming that these photons pass through the spherical surface through a solid angle $d\Omega$ subtended by a hole in the cavity; then it is necessary to define the density of states per solid angle as: $D_\Omega(E) = D(E)/4\pi$; where 4π is the maximum value of Ω. Equation(1.1) can therefore be re-written as:

$$\frac{dn(E)}{dE} = D_\Omega(E)f(E)d\Omega = \frac{2d\Omega}{(hc)^3} \frac{E^2}{exp(\frac{E}{kT}) - 1} \tag{1.3}$$

Equation(1.3) is the photon density per energy interval. The energy density per energy interval follows directly from equation(1.3) as:

$$\frac{du(E)}{dE} = ED_\Omega(E)f(E)d\Omega = \frac{2d\Omega}{(hc)^3} \frac{E^3}{exp(\frac{E}{kT}) - 1} \tag{1.4}$$

where $u(E)$ is the energy density of the photons in the cavity in units of J/m^3. Equation(1.4) can be expressed in terms of wavelength as:

$$\frac{du(\lambda)}{d\lambda} = \frac{2d\Omega}{\lambda^5} \frac{hc}{exp(\frac{hc}{\lambda kT}) - 1} \tag{1.5}$$

by making the substitutions $E = hc/\lambda \Rightarrow dE = -hcd\lambda/\lambda^2$, where $h = 4.13 \times 10^{-15}$ eVs is Planck's constant, and λ is the photon wavelength. Equation(1.5) is called the *wavelength spectrum* while the energy density per photon energy $du(E)/dE$ is called the *energy spectrum*. Another useful quantity is the energy current density; $j(E) = u(E)c$ in units of W/m^2. The energy current density per energy interval becomes:

$$\frac{dj(E)}{dE} = \frac{2d\Omega}{h^3c^2}\frac{E^3}{exp(\frac{E}{kT}) - 1} \tag{1.6}$$

Finally, we define the photon flux(*the number of photons leaving the cavity through a solid angle $d\Omega$ per unit area per unit time*) as: $\phi(E) = n(E)c$, so that we can write the photon flux per energy interval as:

$$\frac{d\phi(E)}{dE} = \frac{2d\Omega}{h^3c^2}\frac{E^2}{exp(\frac{E}{kT}) - 1} \tag{1.7}$$

Integrating equation(1.6) from 0 to ∞ leads the to the famous Stefan-Boltzmann law which holds for a planar blackbody emitting photons into the hemisphere of solid angle $\Omega = \pi$, i.e:

$$j(E) = \frac{2\pi}{h^3c^2}\int_0^\infty \frac{E^3dE}{exp(\frac{E}{kT}) - 1} = \frac{2\pi^5(kT)^4}{15h^3c^2} = \sigma T^4 \tag{1.8}$$

where $\sigma = \frac{2\pi^5k^4}{15h^3c^2} = 5.67 \times 10^{-8}W/m^2K^4$ is the Stefan-Boltzmann constant.

1.4 Solar Spectrum

The solar spectrum is split into a spectrum of either energy (E) or wavelength (λ), both being related by the equation:

$$E[eV] = \frac{hc}{\lambda} = \frac{1242}{\lambda[nm]} = \frac{1.242}{\lambda[\mu m]} \tag{1.9}$$

The solar radiation emanating from the sun comprises of photons of different energies and wavelength. Since we are dealing with the band gap of semiconductors, we will adopt the energy units in electron volts(eV) throughout the scope of this study. [2] The radiation pattern on a solar cell is highly dependent upon its location. The solar flux striking a cell lying above the atmospheric layer will be higher than that lying beneath due to absorption

[2]The solar spectrum is described in many solar physics textbooks. What I did in this section was to provide a summarized perspective required for both theoretical and computational modeling of solar cells. The concept is very important as it tells you what your solar cell actually absorbs! Note that AM1.5 is classified into AM1.5D, AM1.5G and so on depending on climatic conditions. The AM1.5G is used throughout this work [17], which I simply call AM1.5.

of some of the photons by molecules in the atmosphere. Due to this, the solar spectrum is classified into three with respect to the thickness, t_0 of the atmospheric airmass(**AM**); which also accommodates for resonant absorption peaks of specific molecules in the atmosphere. The path length t through the atmosphere for radiation from the sun incident at an angle a relative to the normal to the earth's surface is given by: $t = t_0/cosa$. This characterizes the real solar spectrum resulting from the absorption by a layer of air of thickness t. The spectrum outside the atmosphere is called the extraterrestrial spectrum and it is designated as **AM0**. On the surface of the earth for sun rays at normal incidence, the spectrum is designated as **AM1.0**; since $t/t_0 = 1/cosa = 1$.

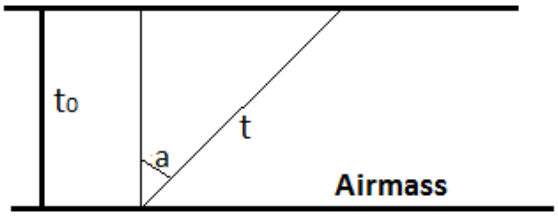

Figure 1.3: Sketch of atmospheric airmass of thickness t_0. The airmass coefficient; t/t_0 depends on the tilt a from the normal.

A typical spectrum for moderate climate is **AM1.5** where, $t/t_0 = 1/cosa = 1.5$ corresponding to an angle of incidence of solar radiation of $a = 48^0$ relative to the surface normal. Both **AM0** and **AM1.5** are terrestrial spectra but **AM1.5** is the standard spectrum for measuring solar cell efficiencies [3].

The integral over the solar wavelength spectrum gives the energy current density onto a surface normal to the sun as:

$$j_{AM1.5}(\lambda) = 2\int_{\lambda_{min}}^{\lambda^{max}} \frac{hc_0{}^2 d\Omega d\lambda}{\lambda^5(exp(\frac{hc_0}{\lambda kT_s}) - 1)} = \int_{\lambda_{min}}^{\lambda^{max}} S(\lambda)d\lambda \approx 1000W/m^2 \equiv 1sun. \quad (1.10)$$

where $S(\lambda)$ is the energy current density of the solar photons per wavelength interval in units of $W/m^2/nm$ also called the *spectral irradiance*, $\lambda_{max} = 4000nm, \lambda_{min} = 280nm$, T_s is the temperature of the sun equal to $5800K$, and $d\Omega = \Omega_s$ is the solid angle subtended by the sun.

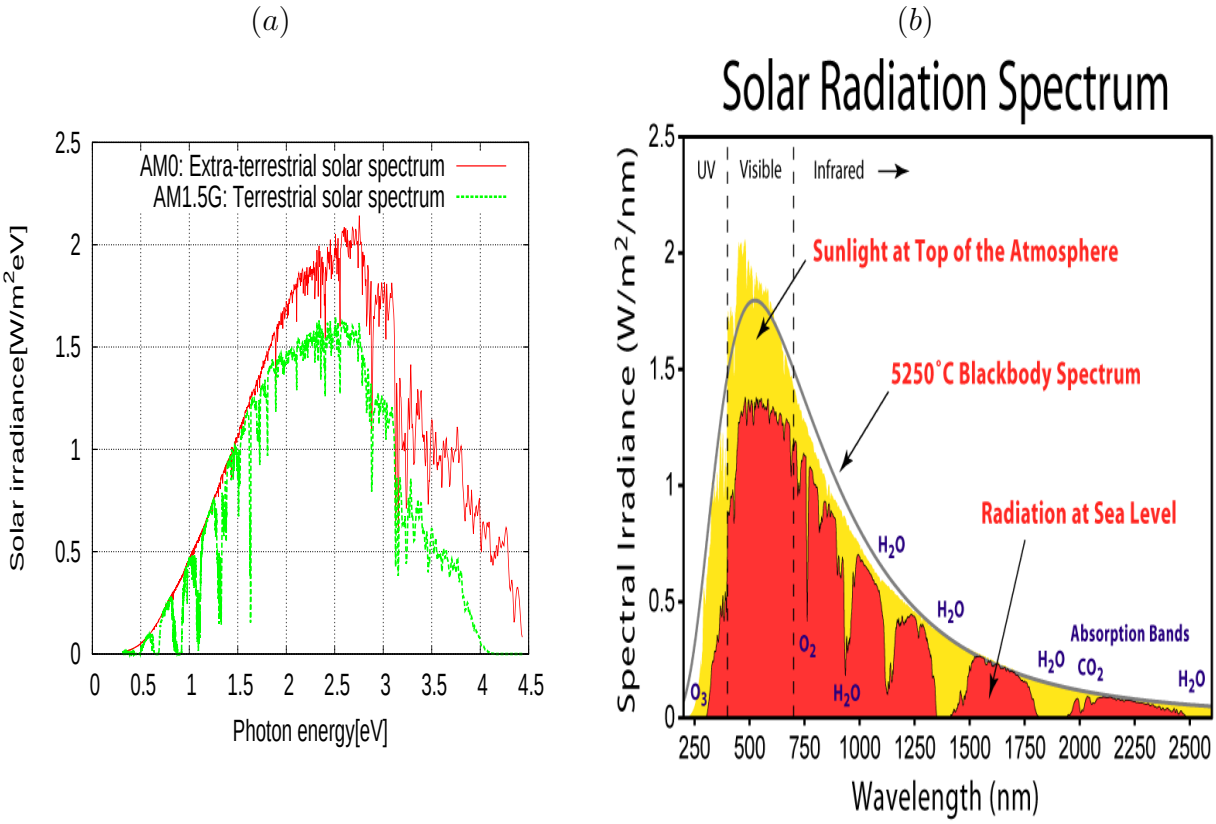

Figure 1.4: The energy spectrum (a) and the wavelength spectrum (b) [17] of the solar terrestrial and extraterrestrial spectra. The visible spectrum which ranges from $1.5eV - 3.0eV$ in the energy spectrum, and from $400nm - 700nm$ in the wavelength spectrum corresponds to the maximum values of solar irradiance.

The absorption of solar radiation is mostly caused by gases such as H_2O, CO_2, and CH_4 in the infrared/below infrared region of the solar spectrum; and in the ultraviolet region by ozone; O_3 and oxygen; O_2 as can be seen in the **AM1.5** wavelength spectrum.

From equation(1.7), we can write the photon flux per wavelength interval as:

$$\frac{d\phi(\lambda)}{d\lambda} = \frac{2c_0 d\Omega d\lambda}{\lambda^4(exp(\frac{hc_0}{\lambda kT}) - 1)} \tag{1.11}$$

Comparing equations(1.10) and (1.11), one arrives at the following very important relationship:

$$\phi(\lambda) = \int_{\lambda}^{\lambda_{max}} [\frac{\lambda}{hc_0}][\frac{dj_{AM1.5}(\lambda)}{d\lambda}]d\lambda \Rightarrow \phi(E) = \int_{E}^{E_{max}} [\frac{hc_0}{E^3}][\frac{dj_{AM1.5}(\lambda)}{d\lambda}]dE \tag{1.12}$$

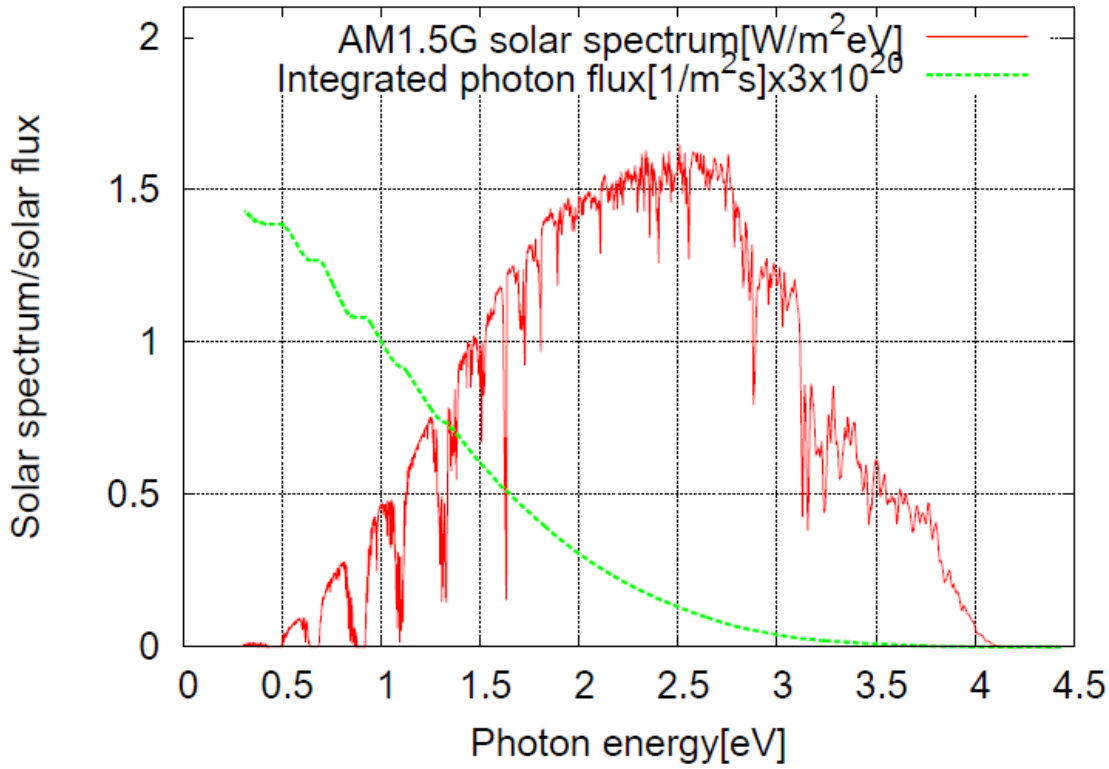

Figure 1.5: Shows the integrated AM1.5G solar flux; eq.(1.12), and the energy spectrum plotted on the same graph.

The importance of Fig.1.5 is that it gives the total number of photons contained in each photon energy emitted from the sun's surface per unit time. For instance, a photon of energy $1.5eV$ contains $0.6 \times 3 \times 10^{20}$ photons per m^2 per second. This is also one of the reasons semiconductors with band gaps in the range $2.5eV - 4.5eV$ are not used for solar cell applications.

CHAPTER 2

Detailed Balance Theory of a pn junction Solar Cell

> ...every theoretical physicist who is any good knows six or seven different theoretical representations for exactly the same physics.
>
> **Richard Feynman**

As with the case of many fields in physics, the efficiency of a solar cell can be derived through different methods. One of those is the detailed balance model, which was first presented in 1961 by Shockley and Queisser, and it has been the standard model for calculating solar cell efficiencies ever since [2, 3, 4]. There are other models such as those based on energy and entropy exchange and those that employ the electron transport equations [10, 11, 12]. However, the detailed balance model is usually preferred because it is relatively simple and insightful, and it requires much less extensive calculations than for example the more realistic models using the electron transport equations. Moreover, it is fundamental and parameter-free.

The detailed balance theory is based on the statistical balance between exciton generation and the possible recombination of the electron and hole within the solar cell. Hence, we can write that:

$$J = q(R_{gen} - R_{rec}) \tag{2.1}$$

where q is the electronic charge, $q = 1.602 \times 10^{-19}C$, R_{gen} is the rate of generation of an electron-hole pair due to the absorption of incident photons from the sun, R_{rec} is the total rate of recombination of the photo-generated carriers, and J is the current extracted from the cell per unit cell area. From this equation, the efficiency of a solar cell can be calculated

as well as the current-voltage characteristics of the cell.

Since the first version was presented in 1961, several authors have extended the detailed balance model [3, 11]. Their main contribution was to remove some approximations that lead to optimistic results. For instance, getting rid of the assumptions that the cell has an infinite dimension with a "step-function absorbance". First, we will obtain the ultimate efficiency limit for a lossless hypothetical solar cell. After this we shall show how from the exact model, one obtains the original model proposed by Shockley and Queisser by using the ideal diode approximation. Finally, the Shockley-Queisser model will be summarized in order to present a detailed perspective based on the strong connection between power conversion efficiency(PCE) of the cell and the band gap of the semi-conducting absorbing layer. Also, the implications of the assumptions made in the detailed balance model will be outlined since we plan to revisit some of them in the later part of this study.

2.1 The Ultimate Limit

To calculate the ultimate efficiency limit η^{ul} for a solar cell with a light absorber of certain cut-off photon energy (in this case given by the band gap energy Eg of the absorber) Shockley and Queisser made the following assumptions:

1. The solar cell has an infinite thickness, and hence an infinite volume.
2. The solar cell consists of a single pn junction as the ideal junction for splitting of $e^{-}h^{+}$ pairs via photon absorption.
3. The cell is lossless; it does not undergo carrier recombination losses($R_{rec} = 0$).
4. Both the solar cell and the sun are blackbodies.
5. Light absorption within the cell follows a step-function:

$$a(E) = \begin{cases} 1, & E \geq E_g \\ 0, & E < E_g \end{cases} \tag{2.2}$$

   where $a(E)$ is the absorbance or absorptivity of the cell which depends on both the photon energy E , the absorption coefficient; $\alpha(E)$ of the absorber, and the absorber thickness, l which in this case, $l \to \infty$. This means that only incident photons with energy, $E \geq E_g$ are absorbed while those with $E < E_g$ are not absorbed(i.e are transmitted)
6. A single $e^{-}h^{+}$ pair is created per absorbed photon and it is extracted at a voltage $V_g = E_g/q$.
7. No optical means is used to concentrate sunlight.

8. An absorbed photon with energy $E > E_g$ does to cause thermalization losses due to its excess kinetic energy which it might deliver to the phonons in the crystal.

The above assumptions leads to the ultimate efficiency limit defined as:

$$\eta^{ul} = \frac{P_{out}}{P_{in}} = \frac{J_{sc}V_g}{j_{AM1.5}} \tag{2.3}$$

where J_{sc} is the photo-generated current density also called the short-circuit current density. The expression for J_{sc} follows from eq.(1.12) with the modifications $\lambda = hc_0/E$, $d\lambda = -hc_0dE/E^2$, and $R_{gen} = \phi(E)$ as:

$$J_{sc} = qR_{gen} = q\int_{E_{min}}^{E_{max}} a(E)\phi_{sun}(E)dE = q\int_{E_g}^{E_{max}} [\frac{hc_0}{E^3}][\frac{dj_{AM1.5}(\lambda)}{d\lambda}]dE. \tag{2.4}$$

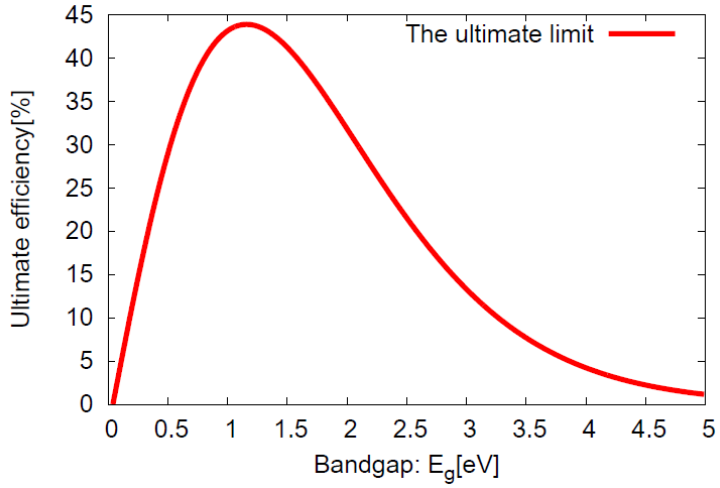

Figure 2.1: The ultimate efficiency as a function of the semiconductor band gap. The peak of the curve corresponds to the optimal value of the ultimate efficiency. This gives an optimum value of $\eta^{ul} = 44\%$ at $E_g = 1.17eV$. η^{ul} goes to zero at both $E_g \to 0$ and $E_g \to \infty$ respectively.

2.2 The Solar Cell Equation

In simple terms, a solar cell is not different from a pn junction diode under illumination. In order to arrive at such an equation, equation(2.1) needs to be re-visited. To do so, let

us define a term; χ [1] called the *external quantum efficiency(EQE)* of the cell also known as *radiative efficiency* such that:

$$\chi = \frac{R_{rec}^{rad}}{R_{rec}} = \frac{R_{rec}^{rad}}{R_{rec}^{rad} + R_{rec}^{non-rad}} \tag{2.5}$$

Re-arranging equation(2.5) leads to:

$$R_{rec}^{non-rad} = R_{rec}^{rad}\Big(\frac{1-\chi}{\chi}\Big) \tag{2.6}$$

Equation(2.6) allows us to define the *radiative limit* of a solar cell as the limit which corresponds to $\chi = 1$; a situation where all the losses are indeed *radiative*. R_{rec}^{rad} is the recombination rate of free carriers due to radiative losses, i.e the emission of a photon from the cell due electron-hole recombination, $R_{rec}^{non-rad}$ is the total rate of carrier recombination which does not involve the emission of a photon. This can be *Auger recombination*, which occurs when free carriers recombine but instead transfers energy to phonons in the crystal, *Shockley-Reed-Hall(SRH) recombination*, which occurs when free carriers are trapped within the crystal due to voids arising from crystal defects, or *thermalization losses*, which occur when high energy photons transfer excess kinetic energy to the crystal lattice. However, in perovskite solar cells, it has been observed that the existence and behavior of Warnier excitons [19] causes radiative losses to dominate [6].

The detailed balance limit also called the Shockley-Queisser limit is a modification of the ultimate limit with two extra basic assumptions considered [2];

1. Radiative loss was considered as the only loss mechanism of photons from the solar cell. The term for radiative recombination from the semiconductor follows from the Van Roosbroeck-Shockley(vRS) relation [16]; which is quite similar to the blackbody radiation but in addition it accounts for the chemical potential; μ of the cell:

$$R_{rec}^{rad} = \frac{2\Omega_c n^2}{h^3 c_0^2}\int_0^\infty e(E)\frac{E^2 dE}{exp(\frac{E-\mu}{kTc}) - 1} \tag{2.7}$$

   where $\mu = qV$; is assumed to be constant throughout the semiconductor, V is the voltage extracted from the cell, T_c is the cell's temperature at 300k,and Ω_c is the solid

[1] Note that this is different from the internal quantum efficiency, IQE defined as a measure of the charge extracted per photon absorbed. It is given by: $\eta_{IQE} = \eta_{ED} \times \eta_{CT} \times \eta_{CC}$, where η_{ED} =exciton diffusion efficiency, η_{CT} =charge transfer efficiency, and η_{CC} =charge collection efficiency. IQE approaching unity implies that almost every photon absorbed is converted to a pair of charge carriers, and that almost all the charge carriers generated are efficiently collected at the positive and negative electrodes. It is entirely material dependent.

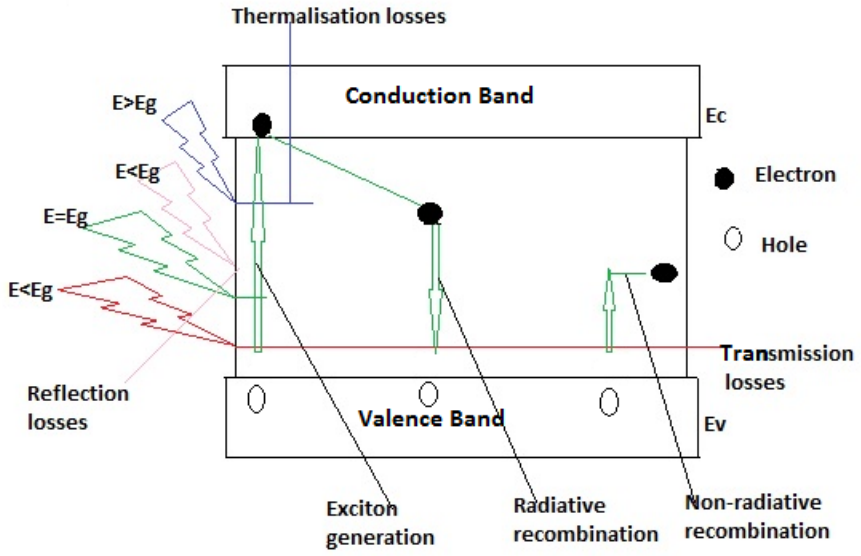

Figure 2.2: Simplified band diagram showing some of the different recombination pathways, carrier generation due to absorption of a green energy photon, blue energy photon create free carriers that thermalize, while purple and indigo photons are either transmitted or reflected. A free electron can also be trapped in a defect site within the absorber and fails to make it to the conduction band.

angle through which photons exit the top surface of the cell; given as $\Omega_c = \pi$ for a planar cell. [2]

2. Kirchorff's law for blackbody radiation holds, i.e the emittance $e(E)$ of the cell is also a step-function as in equation(2.2) both in the dark, and under illumination; where the condition for steady-state is that the total rate of photon emission be the same as the rate at which solar photons are absorbed corrected by the fraction that is drawn off as current in the external circuit.

Hence, substituting equations (2.5),(2.6),and (2.7) into eq.(2.1), and re-writing eq.(2.4) in terms of the blackbody spectrum leads to:

$$J = q(R_{gen} - R_{rec}^{rad} - R_{rec}^{non-rad}) \tag{2.8}$$

[2]Its origin is traced back to electron and hole population densities, n and p within the cell; such that the rate of radiative recombination $R_{rec}^{rad} = R_0 np/n_i^2$ where R_0 is the radiative loss for a solar cell in the dark and it is proportional to the Boltzmann factor $exp(-E/kTc)$, and np/n_i^2 is proportional to $exp(\mu/kTc)$, n_i is the intrinsic carrier concentration, and μ is the difference between the quasi-fermi energy levels of the electron and hole respectively. [5, 18, 2, 15] . See section (5.1.3) for the derivation of eq.(2.7) and other required derivations such as for Ω_s and Ω_c .

$$J = q\Big[\frac{2\Omega_s}{h^3c_0^2}\int_0^\infty a(E)\frac{E^2dE}{exp(\frac{E}{kTs})-1} - \frac{2\pi n^2}{\chi h^3c_0^2}\int_0^\infty e(E)\frac{E^2dE}{exp(\frac{E-qV}{kTc})-1}\Big] \tag{2.9}$$

A crucial part in the performance of a solar cell is that the cell voltage, $V_c = kT_c/q$ never approaches the band gap voltage $V_g = E_g/q$, i.e $E_g - qV > kTc$, where V is the voltage extracted from the cell. This is called the *ideal diode approximation*. Hence, we can re-write equation(2.9) as:

$$J = J_{sc} - J_0 exp(\frac{qV}{kT_c}) = (J_{sc} - J_0) + J_0(1 - exp[\frac{qV}{kT_c}]) = J_{sc} + J_0(1 - exp[\frac{V}{V_c}]) \tag{2.10}$$

where we have used that; $J_{sc} - J_0 \approx J_{sc}$ under illumination. J_0 is the dark saturation current density which should be minimized as much as possible in a solar cell. It is given by:

$$J_0 = q\frac{2\pi n^2}{\chi h^3c_0^2}\int_0^\infty a(E)\frac{E^2dE}{exp(\frac{E}{kTc})} = \frac{q}{\chi}\int_0^\infty a(E)\phi_{cell}(E)dE \tag{2.11}$$

in units of mA/cm^2. A solar cell in its radiative limit; where all recombination is indeed radiative will have an χ of unity and hence a low dark saturation current. Equation(2.10) is the solar cell equation.

2.2.1 Short-circuit current

The short-circuit current density J_{sc} in units of mA/cm^2 is the current extracted from the cell per unit area when the solar cell is not matched to an external load or when it is matched to a load with zero resistance. i.e at $V = 0$. It follows directly from equations (2.10), and (1.7); for a blackbody as:

$$J_{sc} = q\int_0^\infty a(E)\phi(E)dE = q\frac{2\Omega_s}{h^3c_0^2}\int_0^\infty a(E)\frac{E^2dE}{exp(\frac{E}{kTs})-1}. \tag{2.12}$$

2.2.2 Open-circuit voltage

The open-circuit voltage defined as V_{oc} in units of volts (V) is the voltage extracted from the cell when it does not deliver current to an external circuit or when it is matched to a load with an infinite resistance i.e at $J = 0$. Thus, setting $J = 0$ in equation (2.10) leads to:

$$V_{oc} = V_c \ln(\frac{J_{sc}}{J_0} + 1) \tag{2.13}$$

where $V_c = kT_c/q$ is the cell's thermal voltage. The first option to increase V_{oc} is to lower J_0 by changing the spectral shape of $a(E)$: the sharper the step shape the higher the V_{oc}. The

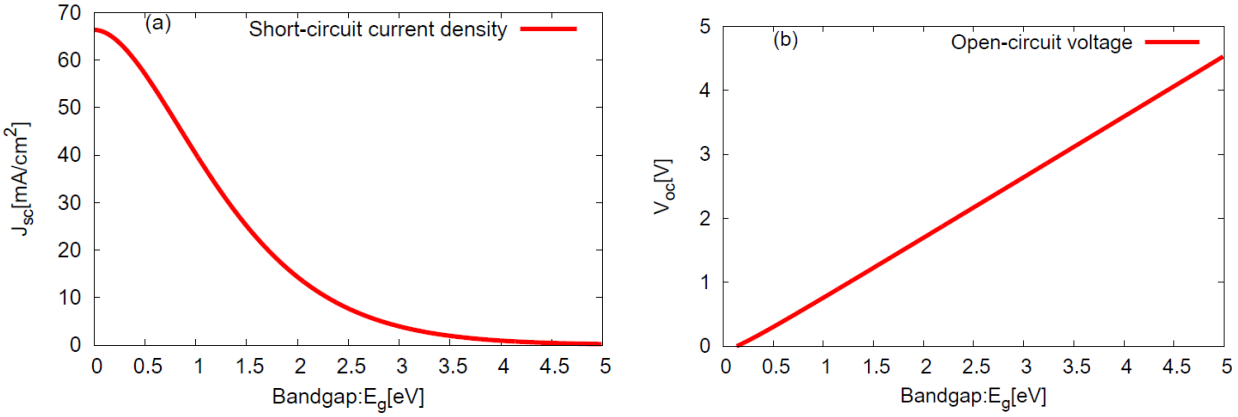

Figure 2.3: (a): Short-circuit current density as a function of the semiconductor band gap. Low band gap semiconductors give higher values of short-circuit current; which decreases with increasing band gap. (b): Open-circuit voltage as a function of the semiconductor band gap. It increases with increasing band gap. Note that it is never equal to the band gap voltage due to *potential loss*.

only other, and more potent option to increase the V_{oc} is instead to increase the χ towards unity by minimizing the non-radiative recombination pathways, bringing V_{oc} closer to the radiative limit. The radiative efficiency hence relates to the offset between band gap and open circuit voltage defined by: $V_{Loss} = (E_g/q) - V_{oc}$. This offset is called the *potential loss*.

2.3 Nominal Limit

The *nominal limit* accounts for the inherent radiative recombination of electron-hole pair in calculating the power conversion efficiency of a solar cell. Hence, it is more useful than the ultimate limit. The efficiency of the cell at this limit, called the *nominal efficiency* η^{nl}, is further reduced when the solar cell is matched to an external load. It leads to the definition of the *nominal power point* as: $JV_{oc}|_{V=0}$.
Hence, the nominal power, $P_n = J_{sc}V_{oc}$, and the nominal efficiency becomes:

$$\eta^{nl} = \frac{P_n}{P_{in}} = \frac{1}{P_{in}} J_{sc}V_{oc} \tag{2.14}$$

2.4 Fill factor

In the same eponymous paper is a term called the *impedance matching factor,m* (now called *fill factor, FF*)[1, 6, 7, 8] introduced by Shockley and Queisser to account for the discrepancy

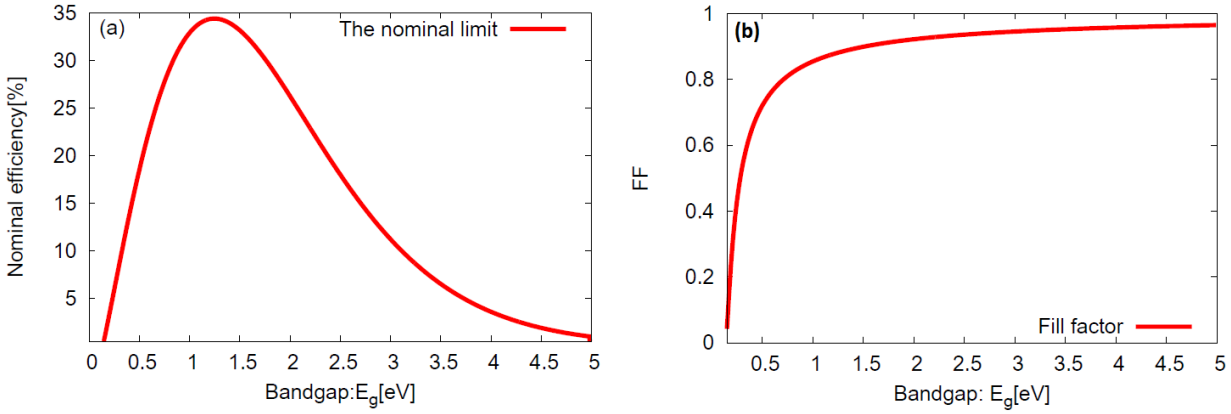

Figure 2.4: (a): The nominal efficiency as a function of the semiconductor band gap. The peak of the curve corresponds to the optimal value of the nominal efficiency. This gives an optimum value of $\eta^{ul} = 34\%$ at $E_g = 1.23eV$. (b): Fill factor as a function of band gap. It rises sharply with band gap but quickly saturates at $E_g \approx 1.50eV$. Values of the fill factor are in the range of $0.80 - 0.90$ in the radiative limit. Note that it never approaches 1.0 except for a lossless cell.

betweeen the power extracted from the cell at both open-circuit and short-circuit conditions; called the *nominal power,*P_n, and the power extracted from the cell when it is *matched* to an external load; called the *maximum power,*P_m. It is an important parameter in solar cell analysis since it tells us by how much P_m approaches P_n, and because it is related to the power conversion efficiency(PCE) of the cell as well as the semiconductor band gap; E_g. Thus, efficient solar cells always have a high fill factor. It is defined as:

$$FF = \frac{P_m}{P_n} = \frac{P_m}{J_{sc}V_{oc}} = \frac{J(V_m)V_m}{J_{sc}V_{oc}} \tag{2.15}$$

where V_m is the voltage extracted from the cell at the maximum power point; $JV \equiv maximum$. Hence, at the maximum power point:

$$d(JV) = 0 \Rightarrow JdV + VdJ = 0 \Rightarrow \frac{dJ}{dV}|_{V=V_m} = -\frac{J_m}{V_m} \tag{2.16}$$

From equations(2.10) and (2.16), we arrive at the expression:

$$\frac{J_0}{V_c}exp(\frac{V_m}{V_c}) = \frac{J_m}{V_m} \Rightarrow J_m = J_0(\frac{V_m}{V_c})exp(\frac{V_m}{V_c}) = J_{sc} + J_0(1 - exp[\frac{V_m}{V_c}]) \tag{2.17}$$

where $J_m = J(V_m) =$ is the current density at the maximum power point. Hence, using optimization techniques the fill factor, FF can be evaluated by optimizing equation (2.15) for V_m.

2.5 The Detailed Balance Limit

The detailed balance limit of efficiency η^{db} also known as the *Shockley-Queisser limit* is the efficiency of the solar cell at the maximum power point. This is the uppermost power conversion efficiency of a hypothetical solar cell with a step-function absorbance, and unity internal quantum efficiency [2]. It is also called the *radiative limit of efficiency* at $\chi = 1$ or the *non-radiative limit of efficiency* at $0 < \chi < 1$. It is defined as:

$$\eta^{db} = \frac{P_m}{P_{in}} = \frac{J_m V_m}{P_{in}} = \frac{1}{P_{in}} FF J_{sc} V_{oc} \tag{2.18}$$

Equation(2.16) can be further re-arranged such that:

$$\eta^{db} = \frac{1}{P_{in} V_g} FF J_{sc} V_g V_{oc} = \eta^{ul} FF \frac{V_{oc}}{V_g} = \eta^{nl} FF \tag{2.19}$$

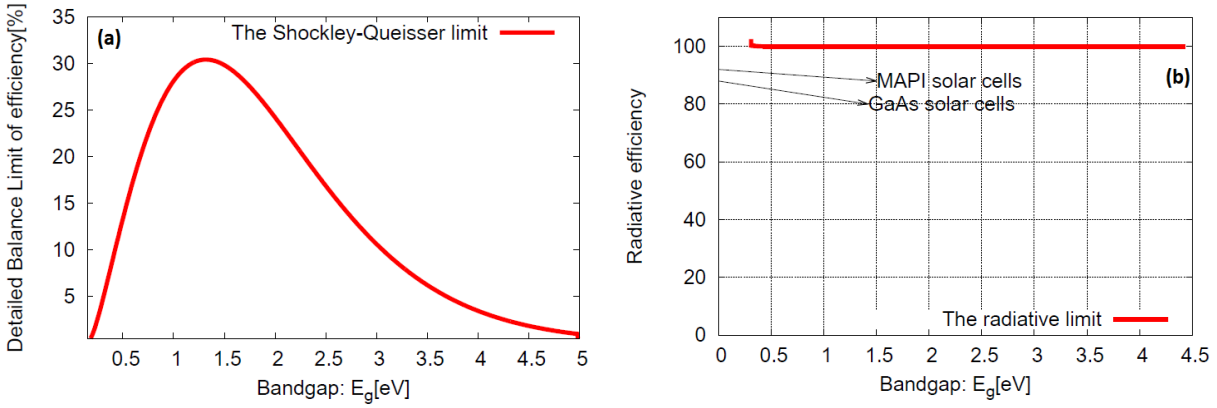

Figure 2.5: (a): The Shockley-Queisser efficiency limit as a function of the absorber band gap. The peak of the curve corresponds to the optimal value of the power conversion efficiency. This gives an optimum value of $\eta^{db} = 30\%$ at $E_g = 1.32eV$. Note that η^{db} goes to zero at both $E_g \to 0$ and $E_g \to \infty$ respectively. (b): The radiative limit at $\chi = 1$ as a function of band gap. The radiative efficiency is $\approx 88\%$ in GaAs ($E_g = 1.42eV$) solar cells, while it is over 90% in MAPI ($E_g = 1.50eV$) cells [6] .

The radiative limit allows us to find an approximate expression for the fill factor as well as most of the important parameters in a solar cell as follows:
First, let us revisit the *meaning* of radiative limit. From equation(2.11) we recognize that at $\chi = 1$:

$$J_0 = J_0^{rad}$$

else

$$J_0 = \frac{J_0^{rad}}{\chi}$$

defines the non-radiative limit

(2.20)

where:

$$J_0^{rad} = q\frac{2\pi n^2}{h^3 c_0^2}\int_0^\infty a(E)E^2 exp(-E/kTc)dE = q\int_0^\infty a(E)\phi_{cell}(E)dE \tag{2.21}$$

Substituting equation(2.20) into (2.13) leads to:

$$V_{oc} = V_c \ln(\frac{\chi J_{sc}}{J_0^{rad}} + 1) \approx V_c \ln(\frac{\chi J_{sc}}{J_0^{rad}}) \tag{2.22}$$

Upon re-arranging, we get that:

$$\chi = \frac{J_0^{rad}}{J_{sc}} exp(\frac{V_{oc}}{V_c}) \tag{2.23}$$

Combining equations(2.22) and (2.17) gives:

$$exp(\frac{V_{oc} - V_m}{V_c}) = 1 + \frac{V_m}{V_c} \tag{2.24}$$

Upon re-arranging, we get that:

$$V_m \approx V_{oc} - V_c \ln(1 + \frac{V_{oc}}{V_c}) \tag{2.25}$$

where we have used $V_m \approx V_{oc}$ inside the logarithm. Hence, equation (2.15) can be re-written as:

$$FF = \frac{J_m}{J_{sc}}[1 - \frac{V_c}{V_{oc}} \ln(1 + \frac{V_{oc}}{V_c})] \tag{2.26}$$

CHAPTER 3

Efficiency Limits of Perovskite Solar Cells

> ..." Our plan was to continuously optimize our perovskite solar cells towards a goal of more than 20% efficiency but these results are ahead of expectations. I see no reason why we can't aim higher now and accelerate the transfer of our technology into production."
>
> **Henry Snaith**

Just as it was mentioned above by the CEO of Oxford PV, the power conversion efficiency(PCE) of perovskite-based solar cells has been continuously optimized from a value of 3.8% [29] since it was first used in 2009 to 9.7% and 10.9% in 2012 [20, 25], 12.0% and 15.4% in 2013 [21, 23], and just recently PCEs of 17.0% [30] and 19.3% [24] were attained. This tremendous rise in PCE in just five years has triggered a lot of active research involving the use of organic-inorganic halide perovskites as light absorbers in solar cells compared to its organic and inorganic counterparts [27].
However, this new, cheap, easy-processable material has some downsides which ranges from low stability and hysteresis losses [7, 21], losses at the hetero-junction interface [8] to Auger and trap-assisted recombinations [30] which generally affect the PCE of the solar cell, in addition to the inevitable radiative recombination [6, 20].

In this chapter, we restrict ourselves to the radiative limit; first with a step-function absorbance, and secondly using the optical absorption spectrum of the three most studied direct band gap halide perovskites; $CH_3NH_3PbI_3$ with a band gap $E_g \approx 1.50eV$ [21], $CH_3NH_3PbI_{3-x}Cl_x$ with a band gap $E_g \approx 1.60eV$ [20], and $CH_3NH_3SnI_3$ with a band gap;

$E_g \approx 1.20eV$ [30] [1] .We will determine the theoretical efficiency limits of these most frequently used active layers in perovskite solar cells.

3.1 Light Absorption in a Perovskite Solar Cell

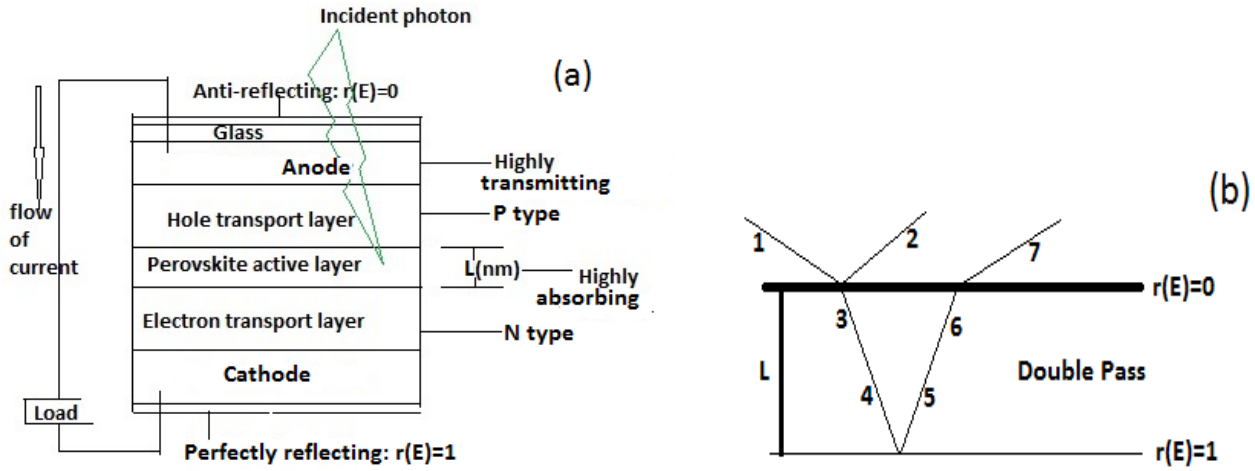

Figure 3.1: The solar cell geometry considered in this study, with zero reflectivity top surface and unity reflectivity back surface. The emitted photons exit the top surface through a solid angle $\Omega_c = \pi$.

Let us denote the incident intensity at the point of contact by: $I(E)$, where $I(E)|_{l=0} = I_0$. This intensity decays as it penetrates through the absorber by an amount:

$$\frac{dI(E)}{dl} = -\alpha(E)I(E) \tag{3.1}$$

where $\alpha(E)$ is the absorption coefficient of the perovskite. Re-arranging and integrating eq.(3.1) gives: $\int \frac{dI(E)}{I} = -\int_0^l \alpha(E)dl \Rightarrow \ln I(E) = -\alpha(E)l + k \Rightarrow k = \ln I_0$. Solving for $I(E)$ leads to:

$$I(E) = I_0 exp(-\alpha(E)l) \tag{3.2}$$

A solar photon with energy E and intensity $I_1(E)$ strikes the top surface of the cell. It is partly reflected as $I_2(E)$ and partly transmitted as $I_3(E)$ eq.(3.1b). The law of conservation of energy requires that: $I_3(E) = I_1(E) - I_2(E)$; where $r(E) = I_2(E)/I_1(E)$ is the reflectance of the top surface. Hence, $I_3(E) = I_1(E) - I_1(E)r(E)$ is absorbed by the perovskite as:

[1] These values are experimental band gaps deduced from the absorption spectra of the perovskites of interest.

$I_4(E) = I_1(E)[1 - r(E)]exp(-\alpha(E)l)$ according to eq.(3.2). The perfect reflector below the cell prevents this from being transmitted, and reflects $I_4(E)$ as $I_5(E)$. It is then re-absorbed as: $I_6(E) = I_1(E)[1 - r(E)]exp(-\alpha(E)l)exp(-\alpha(E)l)$; which finally exists the absorber as: $I_7(E)$.
The total intensity of the absorbed photon becomes:

$$I_a(E) = I_3(E) - I_6(E) = I_1(E)[1 - r(E)] - I_1(E)[1 - r(E)]exp(-2\alpha(E)l) \tag{3.3}$$

$\Rightarrow$

$$a(E) = [1 - r(E)][1 - exp(-2\alpha(E)l)] \tag{3.4}$$

where $a(E) = I_a(E)/I_1(E)$ is the absorbance of the perovskite. We have assumed that the solar cell we are considering is anti-reflecting at the top but perfectly reflecting at the bottom. This allows us to set $r(E) = 0$ from top, and $r(E) = 1$ from below; which ensures that an incident photon is completely absorbed through a distance of $2l$. This leads to the expression:

$$a(E) = 1 - exp(-2\alpha(E)l) \text{ for incident photons through the top.} \tag{3.5}$$

Observe that eq.(3.4) is a modified version of the Bourger's-Beer-Lambert law as it accounts for the double pass due to the reflecting back surface.

3.2 Radiative Limit For Step-Function Absorbance

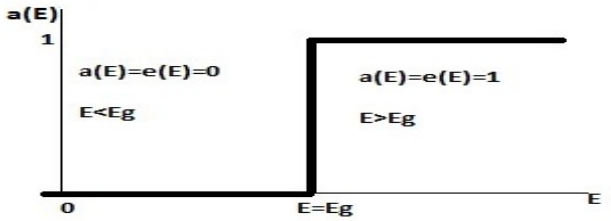

Figure 3.2: Sketch of the step-function absorbance for an ideal absorber. The absorbance of a semiconductor deviates from the ideal. It only approaches the ideal for infinite absorber thicknesses, very high absorption coefficients, and for textured surfaces that allows for light trapping.

Using the step-function absorbance e.q.(2.2), and the AM1.5G solar spectrum fig.(1.4) in place of the blackbody spectrum; the optimum power conversion efficiencies of the three perovskites studied were found only as a function of their band gap.

The optimum values of the short-circuit current density J_{sc}, open-circuit voltage V_{oc}, and the fill factor FF were also determined.

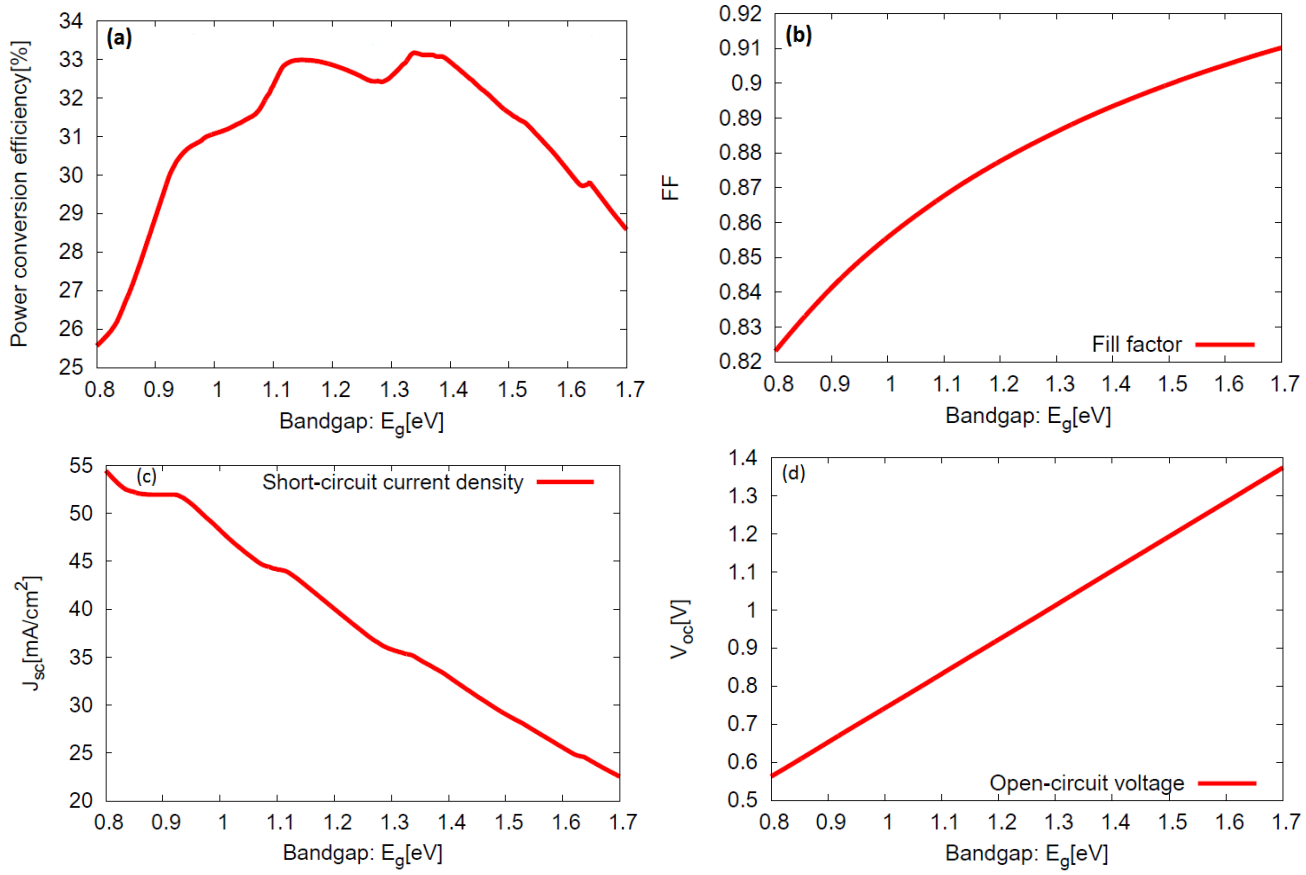

Figure 3.3: (a) The power conversion efficiency limits under AM1.5G solar spectrum as a function of band gap in the range of band gaps of interest (b) Fill factor (c) Short-circuit current density and (d) Open-circuit voltage variation with absorber band gap under AM1.5G solar spectrum with step-function absorbance.

Parameter	$CH_3NH_3SnI_3$	$CH_3NH_3PbI_3$	$CH_3NH_3PbI_{3-x}Cl_x$
$J_{sc}[mA/cm^2]$	40	29	26
$V_{oc}[V]$	0.94	1.20	1.30
FF	0.879	0.900	0.906
$\eta^{db}[\%]$	32.8	31.5	30.0

Table 3.1: Optimal values of the solar cell parameters of interest based on the step-function absorbance.

The importance of table 3.1 is to ward-off against computational errors. The values in the table are valid only for a hypothetical solar cell satisfying all the assumptions in the Shockley-Queisser model. Hence, we expect that real perovskite solar cells will therefore deviate from table 3.1 .

3.3 Radiative Limit For Continuously Varying Absorbance

The active layers in perovskite solar cells can only absorb photons with energy greater than or equal to their band gap, a phenomenon which is very common in inorganic semiconductors. However, to arrive at the most optimistic operating conditions for the solar cell in Fig.3.1; we have made the following assumptions:

1. The solar cell is anti-reflecting for incident photons from the top. Hence, reflection losses are completely eliminated.

2. The internal quantum efficiency(IQE) of the cell is unity; i.e every absorbed photon leads to exciton generation which completely diffuses and gets extracted at the electrodes.

3. Every recombination event produces a luminescent photon which is lost and not re-absorbed; i.e re-generation of free-carriers through absorption of the recombination radiation is not considered.

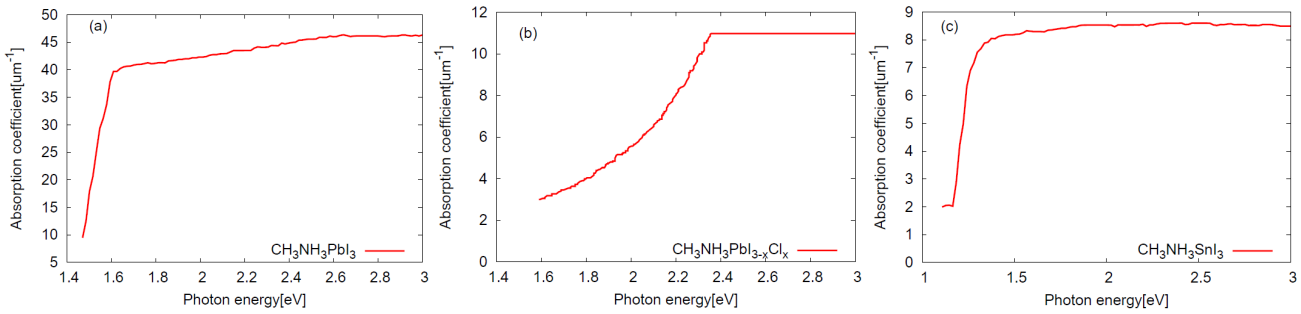

Figure 3.4: The optical absorption coefficients of the perovskites considered at 300K in the vicinity of their band edge. Graphs were reproduced from experimental data: [31],[20], and [29] respectively. The absorption coefficient varies with the energy of the incident photons as: $\alpha(E) = \left(A + \frac{B}{E}\right)(E - E_g)^{\frac{1}{2}}$ [29], where A and B are absorption constants, and E_g is the absorber bandgap.

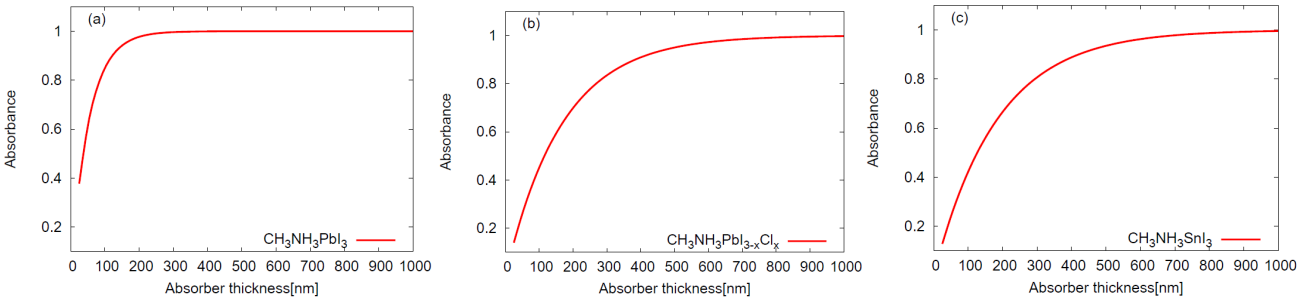

Figure 3.5: Absorbance as a function of thickness for the perovskites considered based on Fig.(3.4).

3.4 Excitons revisited

Having mentioned earlier that the photo-excited carriers in perovskites can be treated in the same manner as with inorganic semiconductors due to the presence of Wannier-type excitons in both materials, it is pertinent to recognize that the exciton diffusion lengths are quite dissimilar [2] , and therefore demands some careful consideration.

The ideal condition would have been that all the charge carriers produced by the absorption of photons should flow towards the electrodes. Unfortunately, the electrons and holes recombine after a lifetime and must be able to reach the electrodes in this time. To see how far an exciton can travel (i.e after separation into free carriers by the in-built electric field in the absorber) by diffusion before it vanishes by radiative recombination, we consider

[2]For instance, the exciton diffusion length in silicon is up to $100\mu m$, with exciton lifetime in the order of $1\mu s$. [5]

a simplified example as shown. Under illumination, an electron is injected into the p-type absorber($CH_3NH_3PbI_3$) as a minority charge carrier. The electron will move in the positive x-direction (i.e towards the electron transport layer).

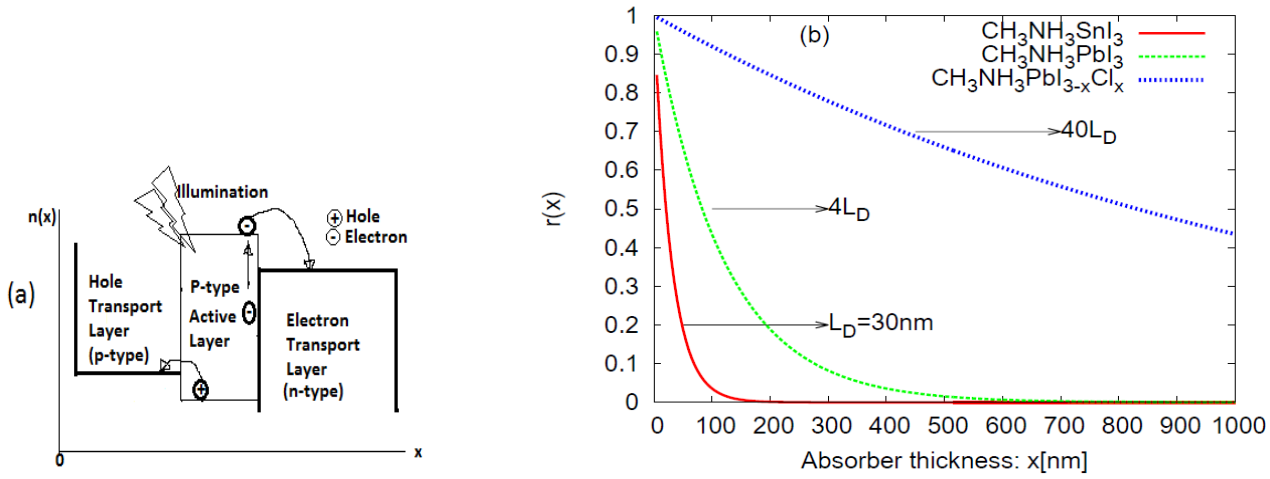

Figure 3.6: (a): a sketch of carrier diffusion process in a p-type perovskite active layer. The minority carrier (electron) moves to the electron transport layer after being injected into the active layer by illumination, hence, an electric field is established in the absorber. (b): The plot of $r(x) = \frac{\Delta n(x)}{\Delta n(0)} = exp(-x/L_D)$ against x (taken as the absorber thickness). It shows how the minority carriers decay in each perovskite absorber. Thick absorbers are disadvantageous for exciton dissociation and carrier transport. Recombination reduces the charge current only if it affects the minority carriers produced by the illumination.

The distribution of the injected electron in the x-direction is given by the diffusion equation:

$$J_n = -D_n \frac{dn(x)}{dx} \qquad \text{and} \tag{3.6}$$

the continuity equation:

$$\frac{\partial n(x)}{\partial t} + \frac{dJ_n}{dx} = G_n - R_n \tag{3.7}$$

where J_n is diffusion current density, $n(x)$ is the electron concentration, D_n is the electron diffusivity, G_n and R_n are the rate of generation and recombination of the electron respectively.

Under illumination, $G_n = G_n^0 = \frac{n^0}{\tau_n}, R_n = \frac{n(x)}{\tau_n} = R_n^0 + \Delta R_n = \frac{n^0}{\tau_n} + \frac{\Delta n(x)}{\tau_n}$, where n^0 is the equilibrium concentration, τ_n is the diffusion lifetime, and $\Delta n(x)$ is injected electron due to illumination. At steady-state, $\frac{\partial n(x)}{\partial t} = 0$. Hence eq.(3.7) reduces to:

$$\frac{dJ_n}{dx} = G_n - R_n = -\frac{\Delta n(x)}{\tau_n} \tag{3.8}$$

and eq.(3.6) becomes:

$$\frac{dJ_n}{dx} = -D_n \frac{d^2 n(x)}{dx^2} = -D_n \frac{d^2 \Delta n(x)}{dx^2} \tag{3.9}$$

Combining(3.8) and (3.4), and re-arranging leads to:

$$\frac{d^2 \Delta n(x)}{dx^2} - \Delta n(x) \frac{1}{\tau_n D_n} = 0 \tag{3.10}$$

Solving for $\Delta n(x)$ leads to:

$$\Delta n(x) = \Delta n(0) exp(-\frac{x}{\sqrt{\tau_n D_n}}) = \Delta n(0) exp(-\frac{x}{L_n}) \tag{3.11}$$

where we have taken the part of the solution that decays with increasing value of x. From eq.(3.11), we observe that: $L_n = \sqrt{\tau_n D_n}$ is the minority carrier diffusion length; (electrons in this case). The diffusivity D_n is related to the carrier mobility μ_n by the Einstein relation: $D_n = \frac{\mu_n kT}{q}$. This relation also holds for holes with n replaced by p.

Perovskite	$L_D(nm)$	$D(cm^2 s^{-1})$	$\tau_D(ns)$	*minority carrier*
$CH_3NH_3PbI_3$	129	0.017	9.79	Electrons
$CH_3NH_3PbI_{3-x}Cl_x$	1213	0.054	272.48	Holes
$CH_3NH_3SnI_3$	30	0.045	0.2	Electrons

Table 3.2: The perovskites of interest and the minority carrier diffusion lengths, diffusivity, and lifetimes [39] and [29]. Error bounds have been neglected. τ_D was calculated from $L_D = \sqrt{\tau_D D}$. In an illuminated cell, only those electrons (or holes) generated in the p-type (or n-type) will reach the n-type (or p-type) at a distance $x \leq L_D$. This becomes very crucial in choosing absorber thicknesses for solar cell applications.

CHAPTER 4

Results and Discussion

4.1 Radiative Limit at an optimum thickness

So far, we have seen that the Shockley-Queisser model does not provide any information concerning the absorber thickness l as well as exciton diffusion length L_D. In this chapter, we discuss the various dependencies of the different solar cell parameters on absorber thickness. The optimum results are found to deviate greatly from experiment, and the reasons for these deviations are discussed.

4.1.1 Short-circuit Current density

At short-circuit condition, a solar cell should experience little or no recombination (i.e $J_{sc} - J_0 \approx J_{sc}$), since it delivers current to a load of zero resistance. The absorber thickness affects J_{sc} in one very important way. Efficient light absorption demands thicker absorbers Fig.(3.4). Hence we observe high short-circuit current in $CH_3NH_3SnI_3$ approaching the Shockley-Queisser Limit(SQL) compared to $CH_3NH_3PbI_3$ and $CH_3NH_3PbI_{3-x}Cl_x$. In each of the halide perovskites, we observed that the thicker the absorber, the higher the J_{sc} which approaches its own SQL. The converse is the case for thinner absorbers, The reason for this is that charge collection at short-circuit is always assisted by the electric field in the absorber, thus the impact of L_D on J_{sc} is rather small. Hence, high J_{sc} is easily obtained in practice.

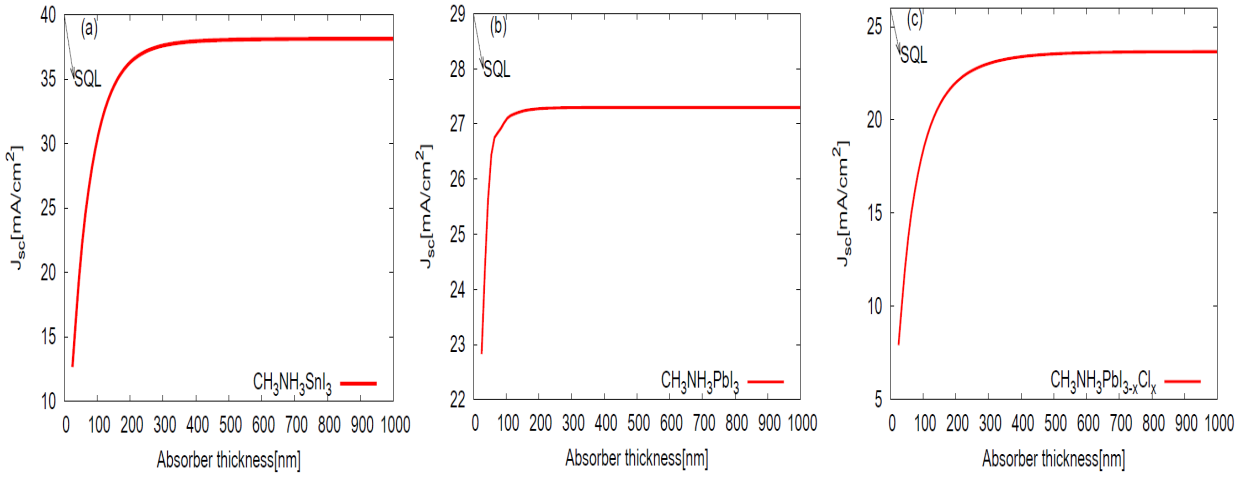

Figure 4.1: Short-circuit current density variation with absorber thickness for each of the perovskite studied.

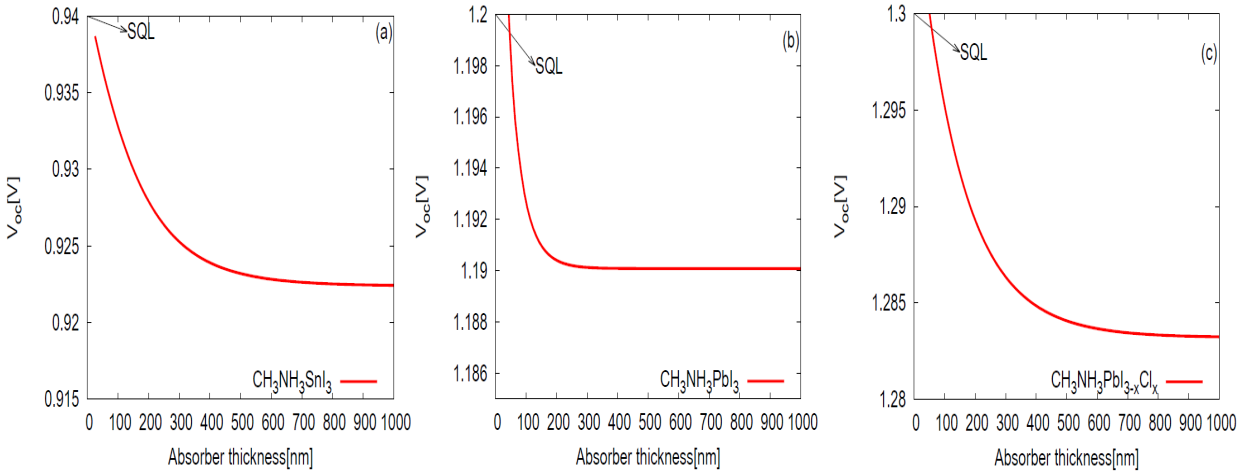

Figure 4.2: Open-circuit voltage variation with absorber thickness.

4.1.2 Open-circuit Voltage

With a load of infinite resistance, a solar cell ends up at V_{oc} and no external current is allowed to flow. Hence, all free carriers generated must also recombine. Hence, the best absorber; generating the highest V_{oc} will be the one where the absorbed photon flux equals the emitted flux under open-circuit conditions. Our results show that thinner absorbers give the highest V_{oc} approaching the SQL. We must *emphasize* though, that the potential loss; $V_{oc}^{SQL} - V_{oc}(l)$ is rather insignificant; which is expected in the radiative limit. Hence, V_{oc} has a weak dependence on absorber thickness and on the exciton diffusion length , since it has a stronger dependence on absorber band gap in accordance with detailed balance

theory. Hence, we can easily infer that higher open-circuit voltages will always be observed in $CH_3NH_3PbI_{3-x}Cl_x$ compared to $CH_3NH_3SnI_3$ and $CH_3NH_3PbI_3$.

4.1.3 Fill Factor

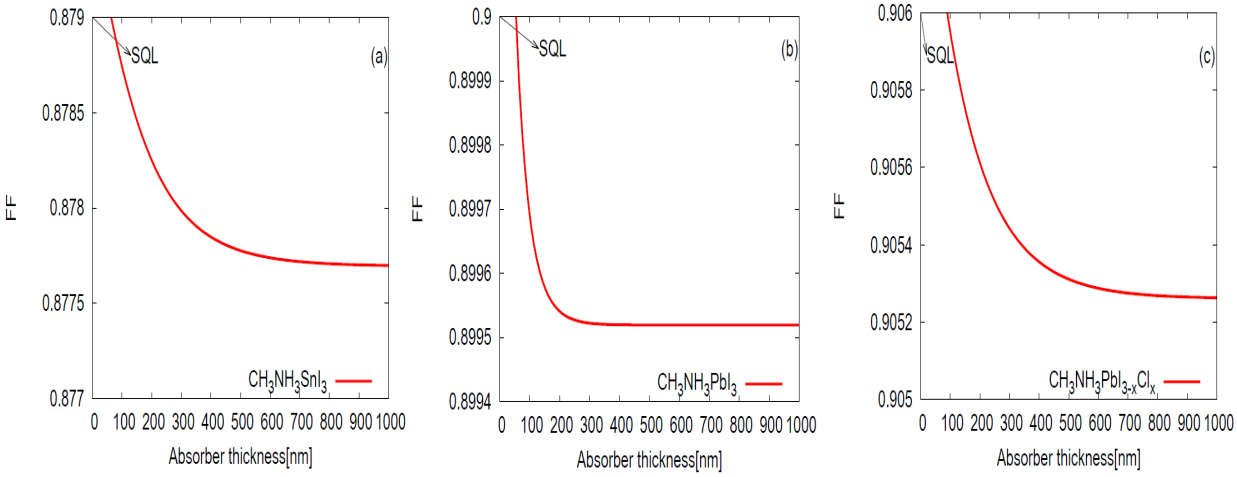

Figure 4.3: Variation of fill factor with absorber thickness.

There is a quick drop in FF as we move away from thinner absorbers, which is more predominant in $CH_3NH_3PbI_3$. Also, the saturation point is quickly reached in $CH_3NH_3PbI_3$, while it takes thicker absorbers to achieve saturation in FF for $CH_3NH_3SnI_3$ and $CH_3NH_3PbI_{3-x}Cl_x$; Fig.(4.3). This is one factor that the FF and V_{oc} also have in common besides their dependence on L_D which is stronger in FF. The reason for this is that the electric field created in the absorber upon illumination decreases with increasing forward bias, and collection of photo-generated carriers which was initially assisted by the electric field, becomes weaker. In general, high FF requires a high quality absorber. Thus, we have the highest FF values in $CH_3NH_3PbI_{3-x}Cl_x$.

4.1.4 Efficiency

The variation of η^{RL}(RL: radiative limit) with the absorber thickness depends on the $J_{sc}(l)$, $V_{oc}(l)$, and $FF(l)$, (i.e $\eta^{RL}(l) = J_{sc}(l) \times V_{oc}(l) \times FF(l)$). The results show that thicker absorbers give high efficiencies. However, we must *emphasize* that the efficiency saturates within the range $l = 300nm$-$400nm$ in each absorber. We also recall that thick absorbers are not good for the FF. Hence, a reasonable conclusion on the behavior of $\eta^{RL}(l)$ must take into account table (3.2),Fig.(3.5), and Fig.(3.6). In view of this, I came up with two

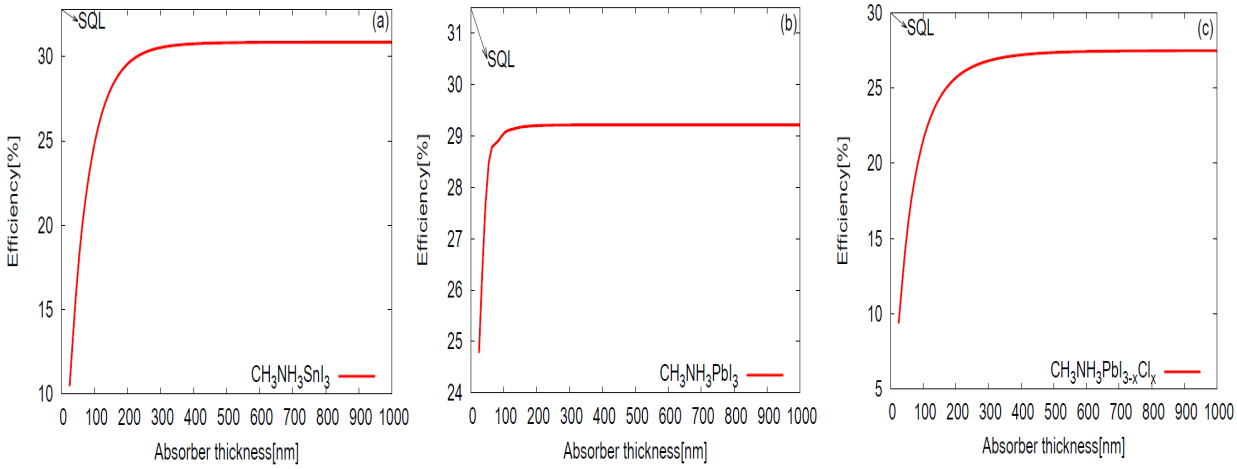

Figure 4.4: Dependence of the power conversion efficiency on the absorber thickness.

tables: one based on *efficient light extraction* using thicker absorbers, and the other based on *efficient charge extraction* using thinner absorbers.

Parameter	$CH_3NH_3SnI_3$	$CH_3NH_3PbI_3$	$CH_3NH_3PbI_{3-x}Cl_x$
$E_g[eV]$	1.20	1.50	1.60
$l[nm]$	400	300	1000
$J_{sc}[mA/cm^2]$	37.94	27.29	23.66
$V_{oc}[V]$	0.924	1.190	1.280
FF	0.8778	0.8995	0.9050
$\eta^{db}[\%]$	30.76	29.20	27.48

Table 4.1: Optimal values of the solar cell parameters of interest based on efficient light absorption.

Parameter	$CH_3NH_3SnI_3$	$CH_3NH_3PbI_3$	$CH_3NH_3PbI_{3-x}Cl_x$
$E_g[eV]$	1.20	1.50	1.60
$l[nm]$	100	200	1000
$J_{sc}[mA/cm^2]$	30.29	27.29	23.66
$V_{oc}[V]$	0.933	1.190	1.280
FF	0.8787	0.8995	0.9050
$\eta^{db}[\%]$	24.82	29.20	27.48

Table 4.2: Optimal values of the solar cell parameters of interest based on efficient charge extraction.

4.2 Theory versus experiment

The fact that the halide perovskites are stable in dry ambient air(with the exception of $CH_3NH_3SnI_3$ [29]), and can be deposited by low-cost solution processing [34] have opened up new avenues for future development of high efficiency, low-cost photo-voltaic cells. It is encouraging to realize how far experimentalists have gone by allowing their device to operate at one sun and without using anti-reflection coatings. For instance, in $CH_3NH_3PbI_{3-x}Cl_x$; V_{oc}, J_{sc}, FF, and η in the range $1.06V - 1.13V$, $19.9mA/cm^2 - 22.8mA/cm^2$, $0.6544 - 0.7536$, and $13.8\% - 19.3\%$ respectively have been reported for absorber thicknesses in the range $200nm - 2\mu m$ [24] . Notice that the V_{oc} and J_{sc} reported approaches the the upper limit Figs.(4.1,4.2). However, V_{oc}, J_{sc}, FF, and η with values $1.07V$, $21.50mA/cm^2$, 0.68, and 15.40% respectively, have also been reported with absorber thickness of $465nm$ [28].

In $CH_3NH_3PbI_3$, V_{oc}, J_{sc}, FF, and η with values $1.08V$, $18.90mA/cm^2$, 0.55, and 11.20% respectively, have also been reported for absorber thickness of $250nm$ [6] . V_{oc}, J_{sc}, FF, and η with values $0.80V$, $17.70mA/cm^2$, 0.62, and 8.70% respectively have also been reported for absorber thickness of $450nm$ [22]. In perovskite solar cells that use $CH_3NH_3PbI_3$ as both a hole transporter and an absorber, V_{oc}, J_{sc}, FF, and η with values $0.631V$, $16.10mA/cm^2$, 0.57, and 5.50%, and $0.905V$, $17.80mA/cm^2$, 0.65, and 10.49%, respectively have also been reported with absorber thicknesses $\leq 400nm$ [34] and [25] .

In $CH_3NH_3SnI_3$, V_{oc}, J_{sc}, FF, and η with values $0.88V$, $16.80mA/cm^2$, 0.42, and 6.00% respectively, have been reported for absorber thickness of $400nm$ [29] . This result reveals the role which exciton diffusion length plays on charge extraction in $CH_3NH_3SnI_3$ since FF and η are far beyond the upper limit. However, the low stability of the Sn^{2+} ion, and non-radiative recombination are also responsible for poor performance of the $CH_3NH_3SnI_3$ absorber.

CHAPTER 5

Conclusion and Recommendation: Beyond the Current Limit

Using a modified version of the Shockley-Queisser model that depends on a continuously varying absorbance, absorber thickness, and anti-reflecting capabilities; we have succeeded in developing the most optimistic operating conditions for the three most widely used perovskite absorbers by purely working in the radiative limit. This led us to the definition of radiative efficiency as a key figure of merit that provides information on how far a solar cell is from its own upper limit.

First, we observed that if the absorber is too thin, then it will not absorb sufficient sunlight. This effect is observed to be more predominant in $CH_3NH_3SnI_3$ and $CH_3NH_3PbI_{3-x}Cl_x$ than in $CH_3NH_3PbI_3$. Hence, for efficient light absorption, thicker absorbers should be used in $CH_3NH_3SnI_3$ and $CH_3NH_3PbI_{3-x}Cl_x$ based solar cells in order to achieve high J_{sc} and V_{oc}. On the other hand, we observed that if the absorber is too thick, charge extraction will be generally poor. This effect is observed to be more predominant in $CH_3NH_3SnI_3$ and $CH_3NH_3PbI_3$ than in $CH_3NH_3PbI_{3-x}Cl_x$. Hence, for efficient charge extraction, thinner absorbers should be used in $CH_3NH_3SnI_3$ and $CH_3NH_3PbI_3$ based solar cells in order to achieve high FF and η.
However, as will be slightly discussed in this chapter, a more rigorous and generalized approach should not be limited to only the radiative limit.

5.1 Recommendation: Beyond the Current Limit

In real solar cells, non-radiative losses are always encountered. These pathways do not include the emission of a photon and are highly device dependent. For instance, trap-states

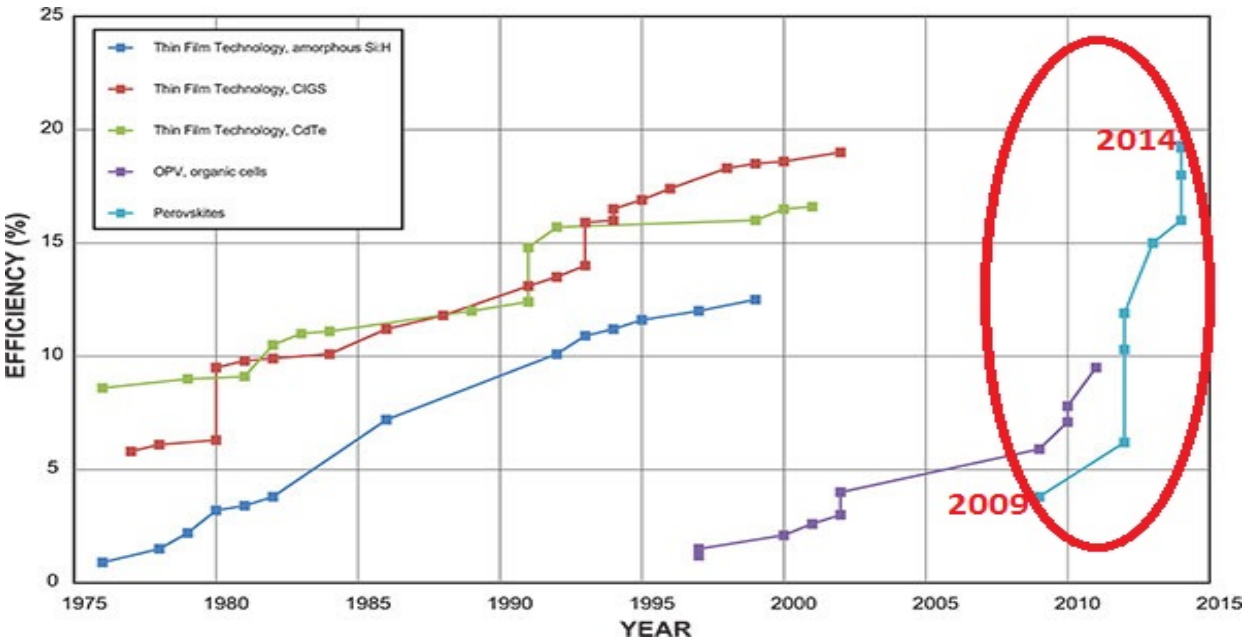

Figure 5.1: [26]Experimental power conversion efficiency limits of different technologies. Perovskites have thin film technologies as its major competitor. Projected values of PCE are up to 20% for perovskite solar cells. Recent laboratory records debut at 17% [30] and 19.3% [24] respectively.

and defects have been detected and studied in $CH_3NH_3PbI_{3-x}Cl_x$ [20] . They are not needed and should be minimized as much as possible, a task that is generally not easy in practice. For a more rigorous calculation of the theoretical upper limit of efficiency of perovskite solar cells, I propose the inclusion of either one or more of the following non-radiative pathways:

1. *Free carrier absorption*: An incident photon can be absorbed by a free carrier within the semiconductor. The free carrier in turn dissipates the energy as heat by interacting with the phonons in the lattice. To distinguish this from the absorption process $\alpha(E)$ in eq.(3.5) which generates electron-hole pairs, we denote it by: $\alpha_0(E)$. Hence eq.(5.4) can be re-written as:

$$a(E) = \begin{cases} \frac{\alpha(E)}{\alpha(E)+\alpha_0(E)+\frac{1}{4n^2 l}}, & n>1,\ textured\ surfaces \\ 1-exp(-2\frac{\alpha(E)}{\alpha_0(E)}l), & n\geq 1,\ specular\ surfaces \end{cases} \tag{5.1}$$

   in the presence of free carrier absorption. However, the free carrier absorption spectrum can only be determined experimentally.

2. *Auger recombination*: which occurs when free carriers recombine but instead of emitting a photon with a particular energy, the energy is rather transferred to phonons in

the crystal. Auger recombination takes place at a rate given by: [3]

$$R_{Auger} = C_n n^2 p + C_p p^2 n \tag{5.2}$$

where C_p and C_n are Auger coefficients for holes and electrons respectively measured from experiment. n and p are the electron and hole concentration respectively.

3. *Shockley-Reed-Hall(SRH)recombination*: occurs when free carriers are trapped within the voids created by crystal defects in a semiconductor. It takes place at a rate given by: [5]

$$R_{SRH} = \begin{cases} \frac{np - n_i^2}{(n+n_i)\tau_p + (p+n_i)\tau_n}, \ general\ case \\ \frac{qw}{2}\sigma V_{th} N_t n_i exp(\frac{qV}{kT}), \ single\ trap\ level \end{cases} \tag{5.3}$$

The first case holds if a single trap level dominates and assuming that the majority of the recombination takes place in the depletion region. w is the junction width, V_{th} is the thermal velocity of minority carriers, N_t is the trap-density, V is the cell 's output voltage, q is the electronic charge, T is the ambient temperature, σ is the capture cross-sectional area which gives the probability of an electron or hole being captured in a defect state. In the general case, n_i is the intrinsic carrier concentration,τ_p and τ_n are hole and electron lifetimes respectively.

However, in an attempt to overcome the detailed balance limit for a single junction device, Physicists have developed different schemes which show a lot of promise in theory. The challenge so far is the implementation of some these schemes in the laboratory since they have their own limitations. These methods have been applied to silicon [3], GaAs, and CdTe solar cells [14]. They include; *Photon recycling(PR)*: a process which involves the re-generation of an electron-hole pair due to re-absorption of the emitted photon within the cell, *Multiple exciton generation(MEG)*: this involves the creation of two or more electron-hole pairs by a single incident photon. The chances of this occurring increases if the energy of the incident photon, $E \geq 3E_g$ where E_g is the absorber band gap. [2][4]. Other methods include; *Photon down conversion,(DC)*, *Photon up conversion(UC)*, *Solar concentration(SC)*, and the use of *multi-junctions* or *tandem cells* [37] . In perovskite solar cells, *mesoscopic structures* have also been used. [34][29] . In this structure; mesopores(nanosize pores)are created on the the electron transport material(ETM) and perovskite nano-particles are allowed to infiltrate into the pores. This is an attempt to enhance electron transport and extraction. We now proceed to discuss a few of these schemes.

5.1.1 Light Trapping

It is possible to increase the absorbance in materials with refractive index $n > 1$ by texturing the surfaces [3]. In this case, incident light is deflected away from the angle of incidence

at one or both interfaces and it is trapped inside the material until is either absorbed or scattered back into the escape cone. The light trapping effect increases the mean path length for a light ray inside the absorber from $2l$ to $4n^2l$ [9][37]. It follows that the probability per unit internal path length for a photon to be absorbed is a ratio of the competing rates; namely the rate at which absorption takes place divided by the rate at which absorption plus escape through the loss cone take place. The absorbance is therefore:

$$a(E) = \begin{cases} \frac{\alpha(E)}{\alpha(E)+\frac{1}{4n^2l}}, & n>1,\ textured\ surfaces \\ 1-exp(-2\alpha(E)l), & n\geq 1,\ specular\ surfaces \end{cases} \tag{5.4}$$

5.1.2 Plasmonic structures

A plasmon is a collective oscillation of the conduction electrons. The idea behind plasmonic structures is to minimize some of the drawbacks mentioned earlier. For example, in [36], Copper nano-plasmonic structures were used to enhance exciton generation in a halide perovskite absorber while simultaneously reducing the film thickness of the perovskite. Two degenerate transverse plasmon modes are supported by two-dimensional ordered Copper nano-plasmonic structure embedded in the absorber. Excitons were effectively generated at the interface between Copper and the absorber. Copper nano-plasmonic structures could reduce the absorber thickness from $400nm$ to $300nm$ while keeping the absorption strength.

5.1.3 Oxide Perovskites

An unexplored class of absorbers for high efficiency solar cells include oxide heterostructures of transition metal oxides with a perovskite structure. Example: $LaVO_3$ grown on $SrTiO_3$ has a direct-band gap of $1.1eV$ [38]. Hence, photons carrying the band gap energy can create electron-hole pairs without the aid of phonons or another indirect scattering processes. The optical absorption of $LaVO_3|SrTiO_3$ over the solar spectrum is comparable to CdTe; a direct band gap material currently used for high-efficiency thin film solar cells.

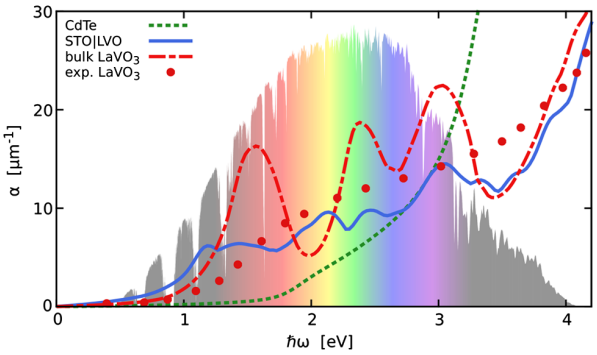

Figure 5.2: The lines show the absorption coefficients of bulk $LaVO_3$ and $LaVO_3|SrTiO_3$ compared to experimental data on bulk $LaVO_3$ and a calculation for CdTe. In the background is $AM1.5$ solar spectrum [38].

Appendices

A Derivations

Following eq.(1.2) , let us now look at a situation whereby photons are emitted from a body with a non-zero chemical potential. A good example of such a body is a semiconductor. [2, 3, 5]. The photon density per energy interval follows from eq.(1.3) but with $f(E,0)$ replaced by $f(E,\mu)$ as:

$$\frac{dn(E)}{dE} = D_{\Omega_c}(E)f(E,\mu)d\Omega_c = \frac{2d\Omega_c}{(hc)^3}\frac{E^2}{exp(\frac{E-\mu}{kT_c})-1} \tag{5.5}$$

$\Rightarrow$

$$\frac{d\Phi(E)}{dE} = c\frac{dn(E)}{dE} = cD_{\Omega_c}(E)f(E,\mu)d\Omega_c = \frac{2d\Omega_c}{h^3c^2}\frac{E^2}{exp(\frac{E-\mu}{kT_c})-1} \tag{5.6}$$

defines the emitted photon flux per energy interval. Ω_c is the solid angle through which photons exit the top surface of the semiconductor, T_c is the temperature of the cell. The angle θ called the *limiting angle of restriction* for the emission of photons lies within $0 \leq \theta \leq \pi/2$ fig.(5.3a), while the azimuth angle ϕ lies within $0 \leq \phi \leq 2\pi$. The emitted photon flux follows from the integration of eq.(5.6) as:

$$\Phi(E) = \int_0^\infty e(E) \int \frac{2}{h^3c^2}\frac{E^2 d\Omega_c}{exp(\frac{E-\mu}{kT_c})-1}dE \tag{5.7}$$

The integral on $d\Omega_c$; i.e $\int d\Omega_c = \int_0^{2\pi}\int_0^{\pi/2} sin\theta d\theta' d\phi$, where $d\theta'$ is a projection of $d\theta$ to the horizontal plane; i.e $d\theta' = cos\theta d\theta$. Hence, $\int d\Omega_c$ becomes:

$$\Omega_c = \int_0^{2\pi}\int_0^{\pi/2} sin\theta d\theta' d\phi = \int_0^{2\pi}\int_0^{\pi/2} sin\theta cos\theta d\theta d\phi = 2\pi\Big[\frac{-cos2\theta}{4}\Big]_0^{\pi/2} = \pi$$

Figure 5.3: (a): a planar cell(abfg) emitting photons through the top surface. (b): a solar concentrator focuses sun rays on a planar cell.

Equation(6) can now be re-written as:

$$\Phi(E) = R_{rec}^{rad} = \int_0^\infty e(E)\frac{2\pi}{h^3c^2}\frac{E^2}{exp(\frac{E-\mu}{kT_c})-1}dE \tag{5.8}$$

where $e(E)$ is the emissivity of the planar cell which has a value of unity for a blackbody emitter, and c is the speed of light in the medium.

From fig.(5.3b), the solid angle subtended by the the sun rays at o due to the solar concentrator is [3]:

$$\Omega_s = \frac{base\ area\ of\ the\ cone}{height\ of\ the\ cone\ squared} = \pi\frac{D_s^2}{4d^2} \approx 6.8\times10^{-5}\ steradian$$

where $D_s = 1.39 million\ km$ is the sun's diameter and $d = 149 million\ km$ is the earth-sun distance. The concentration factor f is a dimensionless quantity that defines both the condition for maximum concentration and no concentration of solar radiation. It is defined as:

$$f = \frac{\Omega_c}{\Omega_s C}$$

where C is the solar concentration. It follows that:

$$\begin{cases} f{=}\frac{\Omega_c}{\Omega_s},\ no\ concentration,\ \Rightarrow C_0{=}1\ sun \\ f{=}1,\ maximum\ concentration \Rightarrow \frac{\Omega_c}{\Omega_s C_{max}}{=}1,\ C_{max}{\approx}46{,}000 suns \end{cases} \tag{5.9}$$

B Summary and Outlook

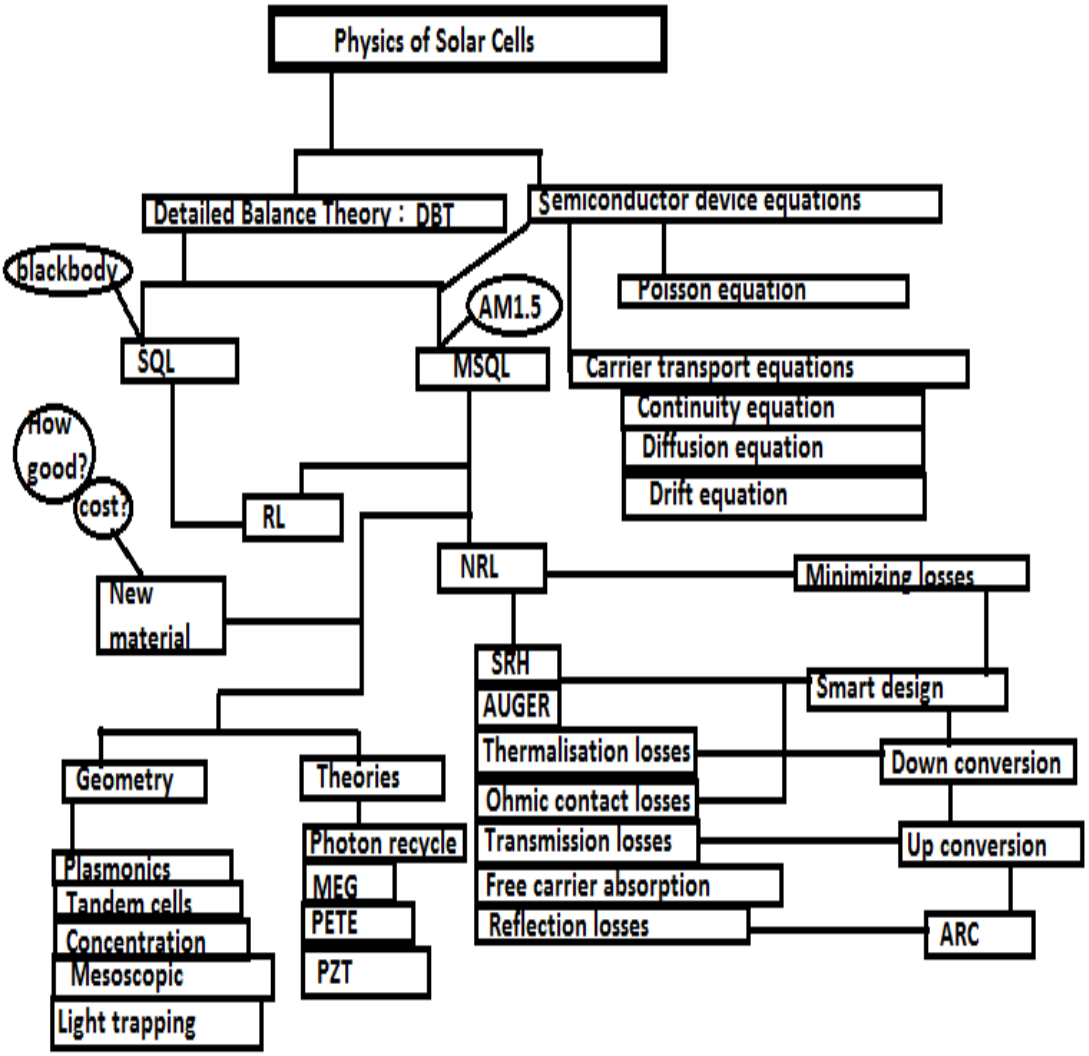

Figure 5.4: RL: radiative losses, NRL: non-radiative losses, ARC: anti-reflection coating, MEG: multiple exciton generation, SQL: Shockley-Queisser limit, MSQL: modified Shockley-Queisser limit, PETE: photon enhanced thermionic emission, PZT: piezoelectric theory.

C Fortran and Octave Codes

```
program flux! calculates solar flux, sf(1/m^2 s)
implicit none! and writes out terrestrial solar irradiance,f(i)(W/m^2 nm)
integer,parameter::nmax=2500
real(8)::et(nmax),ans1,sf(nmax),f(nmax),wl(nmax),E(nmax),ans2,h,c
integer(8)::i
open(40,file='fort.40',status='old')
read(40,*)
do i=1,2002
read(40,*)wl(i),E(i),st(i),et(i),f(i)
end do
!E(i)=Photon energy(eV), wl(i)=wavelength(nm)
!et(i)=AM0, st(i)=AM1.0,f(i)=AM=1.5
h=6.63e-34!h=Planck's constant(Js)
c=3e8 !c=speed of light(m/s)
ans1 = 0.0
do i = 1,2001
ans1 = ans1 + ((f(i) + f(i+1))*(wl(i+1)-wl(i))*wl(i))
sf=ans1/(3*10e20*2.0*h*c*10**9)
write(13,*)E(i),et(i),f(i),sf
end do
end
```

```
clc %calculates solar cell parameters using blackbody spectrum and step-function absorbance
clear all
global kTs kTc wc ws k g
format long E
kTs=0.5168;%in eV
g=15/((kTs * pi)^4);%pre-multiplier
kTc=0.0258;%in eV
wc=pi;%solid angle subtended by the cell
ws=6.85e-5;%solid angle subtended by the sun
k=ws/2*wc;
function temp1=z(E)
global kTs
temp1=E.^2./(exp(E./kTs) - 1);
end
function y=n(Eg)%calculates short-circuit current density
y=quadcc (@z,Eg,inf);
end
```

```
function temp2=h(E)
global kTc
temp2=E.^2./(exp(E/kTc));
end
function d=B(Eg)%calculates dark current density
d=quadcc(@h,Eg,inf);
end
function temp=p(Eg)%calculates open circuit voltage
global kTc k
temp=kTc*log(k*n(Eg)/B(Eg));
end
function temp=ff(Eg)%calculates fill factor
global kTc
vc=kTc;
temp=((p(Eg)/vc)-log(1+(p(Eg)/vc)))/(1+(p(Eg)/vc));
end
function temp3=m(Eg)%calculates detailed balance efficiency
global g
temp3=-n(Eg)*p(Eg)*ff(Eg);
end
pt=fminunc(@m,1.3)
val=-m(pt)*100*g
N=500;
db=zeros(N,1);
Eg=zeros(N,1);%bandgap
for e=1:N
Eg(e)=(e-1)*0.01;
db(e)=-100*g*m(Eg(e));%converts detailed balance efficiency to percentage
end
plot(Eg,db,"pg")
axis([0.1 5 0 40])
xlabel "Solar cell bandgap[ev]";
ylabel "Detailed balance limit of efficiency[%]";
title('The Shockley-Queisser limit')
print("db.pdf", "-dpdf")

program ocv!calculates solar cell parameters using AM1.5 spectrum and step-function absorbance
implicit none
integer,parameter::nmax=2500,pi=3.141592654
```

```
real(8)::d(nmax),f(nmax),wl(nmax),E(nmax),ans,q,ans1,hh,h,c
integer::i
real(8)::wc,vc,Jsc,Jo,Voc,ff,eta1,eta2,eta3,ans2,x,xx,vm,Jm
h=6.63e-34 !Planck's constant in Js
c=3e8 !speed of light in m/s
wc=pi
vc=0.025
q=1.602e-19%electronic charge
hh=4.13e-15 !Planck's constant in eVs
x=1.0! External quantum efficiency
open(17,file='fort.17',status='old')
read(17,*)
do i=1,2001
read(17,*)E(i),wl(i),f(i),d(i)
end do
ans1 = 0.0
do i = 1,2001
ans1 = ans1 + ((f(i) + f(i+1))*(wl(i+1)-wl(i)))
end do
ans1=ans1/2.0 !incident intensity in units of W/m^2 (1 sun)
ans2=0.0
ans=0.0
Jo=0.0
do i=1,2001
ans2=ans2+((d(i) + d(i+1))*(E(i)-E(i+1))*0.5)
Jo=ans2*q*2*wc*0.1/((hh**3)*x*c**2)! dark current density
ans=ans+((f(i) + f(i+1))*(wl(i+1)-wl(i))*wl(i)*0.5)
Jsc=ans*q*0.1/(h*c*10**9)! Short-circuit current density
voc=vc*log((Jsc/Jo)+1) !Open-circuit voltage
vm= voc-vc*log(1+(voc/vc))! maximum voltage
Jm= Jsc+Jo*(1-exp(vm/vc)) !maximum current density
ff=(Jm*vm)/(Jsc*voc)!fill factor
xx=(exp(voc/vc))*(Jo/Jsc)! radiative efficiency
eta1=Jsc*E(i)*100/(0.1*ans1)!ultimate efficiency
eta2=Jsc*Voc*100/(0.1*ans1)!norminal efficiency
eta3=eta2*ff! detailed balance efficiency
write(18,*)E(i),Jsc,voc,ff
write(19,*)E(i),xx,eta1,eta2,eta3
end do
end
```

```
program alll !calculates solar cell parameter for the CH3NH3SnI3 perovskite
!(a similar code is used for the other perovskites studied)
implicit none ! using AM1.5 spectrum and continuously varying absorbance
integer,parameter::nmax=2500
real(8),parameter::c=3e8,wc=pi,pi=3.141592654,vc=0.025 !in eV,hh=4.13e-15 ! in eVs
real(8)::d(nmax),f(nmax),wl(nmax),E(nmax),a(nmax),ans,q,ans1,hh,h,c,ans2,abb
integer::i,t
real(4)::wc,vc,Jsc,Jo,Voc,ff,eta1,eta2,eta3,l,n,ans3,x,vm,Jm,y
q=1.602e-19! electronic charge
ans3 = 1000.2 !incident intensity in units of W/m^2
n=1.0!n=refractive index of absorber
x=1.0!EQE
y=1.0 !IQE
open(58,file='fort.58',status='old')
read(58,*)
do i=1,622
read(58,*)wl(i),E(i),f(i),a(i),d(i)
end do
do t=25,1000,25 !E(i)=photon energy in eV, t=absorber thickness in nm
l=t*0.001 !um !a(i)=absorption coefficient
ans1=0.0 !wl(i)=wavelength
ans2=0.0 !f(i)=AM1.5 solar irradiance in W/m^2/nm
!d(i)=E(i)**2/exp(E(i)/Vc)
do i=1,621 !a(i) is in 1/cm units(convert to 1/um by division by 10000)
abb=1-exp(-2*a(i)*l/10000)!  absorbance ans1=ans1+((f(i)*wl(i)*(1-exp(-2*a(i)*l/10000))
+ f(i+1)*wl(i+1)*(1-exp(-2*a(i+1)*l/10000)))*(wl(i+1)-wl(i)))
ans2=ans2+((d(i)*(1-exp(-2*a(i)*l/10000)) + d(i+1)*(1-exp(-2*a(i+1)*l/10000)))*(E(i)-E(i+1)))
end do
Jsc=(y*ans1*q*0.1)/(2*h*c*10**9) !short-circuit current density
Jo=(ans2*q*2*wc*0.1*n**2)/(2*(hh**3)*x*c**2)!dark current density
voc=vc*log((Jsc/Jo)+1) !open-circuit voltage
vm= voc-vc*log(1+(voc/vc))! maximum voltage
Jm= Jsc+Jo*(1-exp(vm/vc)) !maximum current density
ff=(Jm*vm)/(Jsc*voc)!fill factor
eta2=Jsc*Voc*100/(0.1*ans3)!norminal efficiency
eta3=eta2*ff !Power conversion efficiency
write(64,*)t,abb,Jsc,voc,ff,eta3
end do
end
```

Bibliography

[1] J.Heo et al.
Efficient inorganic–organic hybrid hetero-junction solar cells containing perovskite compound and polymeric hole conductors, nature photonics, doi: 10.1038/nphoton.2013.80,5 MAY 2013.

[2] W.Shockley and H.J. Queisser
Detailed Balance Limit of Efficiency of pn Junction Solar Cells, Journal of Applied Physics 32, 510 (1961); doi: 10.1063/1.1736034.

[3] T.Tiedje et al.
Limiting efficiency of silicon solar cells, IEEE Transactions on electron devices, Vol.ED-35,No. 5, may 1984.

[4] Z.R Abrams et al.
Theoretical efficiency of 3rd generation solar cells: Comparison between carrier multiplication and down-conversion, Solar Energy Materials and Solar Cells (2012), doi:10.1016/j.solmat.2011.12.019.

[5] P.Wurfel
The Physics of solar cells, from principles to new concepts (WILEY-VCH, Berlin;Germany, 2005).

[6] K.Tvingstedt et al.
Radiative efficiency of lead iodide based perovskite solar cells, Scientific reports,4:6071.DOI:10.1038/srep06071, August, 2014.

[7] J.Jeng et al.
*CH3NH3PbI3 Perovskite/Fullerene Planar-Heterojunction Hybrid Solar Cells, Adv. Mater. 2013, 25, 3727–3732.*DOI: 10.1002/adma.201301327 .

[8] H.J. Snaith et al.
Anomalous Hysteresis in Perovskite Solar Cells, American Chemical Society. dx.doi.org/10.1021/jz500113x — J. Phys. Chem. Lett. 2014, 5, 1511−1515.

[9] J. Even et al.
Theoretical insights into multibandgap hybrid perovskites for photovoltaic applications, Photonics for Solar Energy Systems V, Andreas Gombert, Proc. of SPIE Vol. 9140, 91400Y · © 2014 SPIE, doi: 10.1117/12.2052375

[10] T. Kirchartz et al.
Detailed balance theory of excitonic and bulk heterojunction solar cells, Physical Review B 78, 235320, 2008 DOI: 10.1103/PhysRevB.78.235320.

[11] T. Kirchartz et al.
Efficiency limits of organic bulk heterojunction solar cells,J. Phys. Chem. C 2009, 113, 17958–17966, DOI:10.1021/jp906292h.

[12] T. Kirchartz et al.
Charge seperation in organic and bipolar solar cells-A detailed balance approach,Thin Solid Films 516 (2008) 7144 – 7148, doi:10.1016/j.tsf.2007.12.084.

[13] M.C. Scharber, N.S. Sariciftci
Efficiency of bulk-heterojunction organic solar cells,Progress in Polymer Science 38 (2013) 1929–1940 http://dx.doi.org/10.1016/j.progpolymsci.2013.05.001.

[14] O.D. Miller and E.Yablonovitch,
Photon extraction: the key physics to approaching solar cell efficiency limits,EEE Journal of Photovoltaics, 2(3):303–311, 2012.

[15] C. H. Henry
Limiting efficiencies of ideal single and multiple energy gap terrestrial solar cells. Journal of Applied Physics, 51(8):4494–4500, 1980.

[16] W. Van Roosbroeck and W. Shockley,
*Photon-radiative recombination of electrons and holes in germanium.*Physical Review, 94(6):1558–1560, 1954.

[17] AM1.5G solar spectrum
AM1.5 solar spectrum: National Renewable Energy Lab. ASTM G-173-03, Reference Solar Spectral Irradiance: Air Mass 1.5.

[18] P. Wurfel
The chemical potential of radiation. J. Phys. C Sol. Stat. 15, 3967–3985. 1982.

[19] K. Tanaka et al.
Comparative study on the excitons in lead-halide-based perovskite-type crystals CH3NH3PbBr3 CH3NH3PbI3. Solid State Communications 127 (2003) 619–623. doi:10.1016/S0038-1098(03)00566-0.

[20] C. Wehrenfennig et al.
Homogeneous Emission Line Broadening in the Organo Lead Halide Perovskite CH3NH3PbI3−xClx. dx.doi.org/10.1021/jz500434p — J. Phys. Chem. Lett. 2014, 5, 1300−1306

[21] I.C. Smith et al.
A Layered Hybrid Perovskite Solar-Cell Absorber with Enhanced Moisture Stability. Angew. Chem. Int. Ed. 2014, 53, 1 – 5. DOI: 10.1002/anie.201406466.

[22] B. Cohen et al.
Parameters influencing the deposition of methylammonium lead halide iodide in hole conductor free perovskite-based solar cells. APL Materials 2, 081502 (2014); doi: 10.1063/1.4885548.

[23] C. Chen et al.
Efficient perovskite solar cells based on low-temperature solution-processed (CH3NH3)PbI3 perovskite/CuInS2 planar heterojunctions. Nanoscale Research Letters 2014, 9:457. http://www.nanoscalereslett.com/content/9/1/457.

[24] H. Zhou et al.
Interface engineering of highly efficient perovskite solar cells. Science 345, 542 (2014);DOI: 10.1126/science.1254050.

[25] J. Shi et al.
Hole-conductor-free perovskite organic lead iodide heterojunction thin-film solar cells: High efficiency and junction property. Applied Physics Letters 104, 063901 (2014). http://dx.doi.org/10.1063/1.4864638.

[26] C.M. Lampert et al; Science Direct Editorial,
Reporting solar cell efficiencies in Solar Energy Materials and Solar Cells. Solar Energy Materials and Solar Cells 92 (2008) 371–3732 . doi:10.1016/j.solmat.2008.01.003.

[27] S. Sun et al.
The origin of high efficiency in low-temperature solution-processable bilayer organometal halide hybrid solar cells. Energy Environ. Sci., 2014, 7, 399–407 — 399. DOI: 10.1039/c3ee43161d.

[28] M. Liu et al.
Efficient planar heterojunction perovskite solar cells by vapour deposition. Nature.Mater.2013, doi:10.1038/nature12509

[29] N.K. Noel et al.
Lead-free organic–inorganic tin halide perovskites for photovoltaic applications. Energy Environ. Sci., 2014, 7, 3061–3068 — 3061. DOI: 10.1039/c4ee01076k.

[30] C.Wehrenfennig et al.
Charge-carrier dynamics in vapour-deposited films of the organolead halide perovskite $CH_3NH_3PbI_{3-x}Cl_x$. — DOI: 10.1039/c4ee01358a —Energy Environ. Sci., 2014, 7. 2269.

[31] S. De Wolf et al.
Organometallic Halide Perovskites: Sharp Optical Absorption Edge and Its Relation to Photovoltaic Performance. J. Phys. Chem. Lett., 2014, 5 (6), pp 1035–1039; DOI: 10.1021/jz500279b.

[32] T.Minemoto and M.Murata
Device modeling of perovskite solar cells based on structural similarity with thin film inorganic semiconductor solar cells. Journal of Applied Physics 116, 054505 (2014); doi: 10.1063/1.4891982.

[33] C.Chen et al.
Optical Properties of Organometal Halide Perovskite Thin Films and General Device Structure Design Rules for Perovskite Single and Tandem Solar Cells. Department of Materials Science and Engineering, National Tsing Hua University, Taiwan. E-mail: hwlin@mx.nthu.edu.tw.

[34] L.Etgar et al.
Mesoscopic CH3NH3PbI3/TiO2 Heterojunction Solar Cells. dx.doi.org/10.1021/ja307789s — J. Am. Chem. Soc. 2012.

[35] N. Park
Organometal Perovskite Light Absorbers Toward a 20% Efficiency Low-Cost Solid-State Mesoscopic Solar Cell. dx.doi.org/10.1021/jz400892a — J. Phys. Chem. Lett. 2013, 4, 2423−2429.

[36] S. Chang
Plasmonic Structure Enhanced Exciton Generation at the Interface between the Perovskite Absorber and Copper Nanoparticles. http://dx.doi.org/10.1155/2014/128414— Scientific World Journal Volume 2014, Article ID 128414, 6 pages.

[37] B.W. Schneider
Pyramidal surface textures for light trapping and antireflection in perovskite-on-silicon

tandem solar cells. Vol. 22, No. S6 — DOI:10.1364/OE.22.0A1422 — OPTICS EXPRESS A1423.

[38] E. Assmann et al.
Oxide Heterostructures for Efficient Solar Cells. DOI:10.1103/PhysRevLett.110.078701.(2013).

[39] S.D Stranks et al.
Electron-Hole Diffusion Lengths Exceeding 1 Micrometer in an Organometal Trihalide Perovskite Absorber. www.sciencemag.com, SCIENCE, VOL. 342, 18 OCTOBER, 2013.

[40] M. Pope and C.D. Swenberg.
Electronic Processes in Organic Crystals and Polymers. New York University, Oxford University Press, 1999.